Atmospheric sounding of the boundary layer over alpine glaciers using fixed-wing UAVs

Alexander R. Groos^{1,2}, Nicolas Brand², Murat Bronz³, and Andreas Philipp⁴

Correspondence: alexander.groos@fau.de

Abstract.

Glaciers are an integral part of the high mountain environment and interact with the overlying atmosphere and surrounding terrain in a complex and dynamic manner. The energy exchange between the glacier surface and the overlying atmosphere controls ice melt rates and promotes the formation of a low-level katabatic jet that interacts with other, often thermally driven winds in alpine terrain. Information on local circulations and the structure of the atmospheric boundary layer over glaciers is crucial for studying cryosphere-atmosphere interactions and for investigating the characteristics of the katabatic jetwind, its broader cooling effect, and its susceptibility to be broken up disrupted by strong valley or synoptic winds that promote heat advection from the ice- and snow-free periphery towards the glacier. While the number of ground-based measurements from weather stations and meteorological towers installed on glaciers for boundary layer research has increased in recent years, a lightweight and mobile measurement technique for atmospheric sounding over alpine glaciers has not yet been available. Here we describe a new measurement technique based on a low-cost and open-source fixed-wing UAV, which allows sounding the atmospheric boundary layer over glaciers up to several hundred metres above the surface. Vertical In the frame of a feasibility study in 2021, two half-day (16 June, 23 September) and two 24-hour campaigns (9/10 July, 25/26 August), including nocturnal soundings, were performed, demonstrating the UAV's capability to reach heights of up to 800 m above the glacier surface. From these campaigns, 40 profiles of air temperature, humidity, pressure, specific humidity, wind speed, wind direction and turbulence ean be derived from the meteorological and flight recorder data collected by the UAV, and turbulence were derived. The results of a measurement campaign on the Kanderfirn in the Swiss Alps on 16 June 2021 demonstrate the potential of the technique and highlight typical highlight characteristic features of the boundary layer above a melting glacier surface. The soundings reveal a persistent low-level katabatic jet, characterised by a pronounced glacier boundary layer, including a persistent surface-based inversion, relatively dry air, high wind speeds and enhanced turbulence a cool and dry katabatic wind confined to the lowest 50 m AGL, an overlying shear layer, and a warmerand, often more humid valley wind aloftabove 100–200 m AGL. These observations illustrate how the boundary layer structure responds to synoptic forcing and local circulations and demonstrate the potential of UAV-based atmospheric soundings for advancing glacier meteorology in complex alpine terrain.

¹Institute of Geography, Friedrich-Alexander-Universität Erlangen-Nürnberg, 91508 Erlangen, Germany

²Institute of Geography, University of Bern, 3012 Bern, Switzerland

³Fédération ENAC ISAE-SUPAERO ONERA, Université de Toulouse, 31055 Toulouse, France

⁴Institute of Geography, University of Augsburg, 86135 Augsburg, Germany

1 Introduction

55

Glaciers and ice caps are an integral part of the high mountain environment, interacting with the overlying atmosphere and surrounding terrain in a complex and highly dynamic manner. The spatially and temporally highly variable energy exchange between the glacier surface and the overlying atmosphere strongly controls ice melt rates and promotes a characteristic microclimateand, including the formation of katabatic winds, which interact with other, often thermally driven, winds in alpine terrain (e.g. Oerlemans, 2010; Farina and Zardi, 2023). A sound understanding of the principles of multi-scale glacier-atmosphere glacier-atmosphere interactions in alpine terrain and their sensitivity to climate change is essential for accurate and reliable projections of future glacier mass loss (e.g. Mott et al., 2020; Jouberton et al., 2022; Shaw et al., 2023, 2024). Projections of the future evolution of mountain glaciers are, in turn, not only relevant in the context of sea-level rise and freshwater management (e.g. Huss and Hock, 2018; Rounce et al., 2023). They are, but also fundamental for assessing future local changes in the mountain-valley wind system and potential impacts on air temperature and precipitation in glacier forefields related to shrinking ice and snow cover at higher elevations (e.g. Potter et al., 2018; Salerno et al., 2023).

While the general structure of the atmospheric boundary layer over mountain glaciers and the key processes driving the local circulation in glacierised mountain local circulations in glacierised terrain are relatively well understood, less is known about local and regional differences in the manifestation of katabatic winds (depending on glacier characteristicsand the topographic/climatic setting) and their sensitivity to rising air temperatures in ice- and snow-free areas. Both theoretical considerations and glacio-meteorological field experiments have shown that how these circulations vary regionally and how they are modified by glacier characteristics, topography, and synoptic forcing. Katabatic winds, in particular, have been studied extensively, as a melting glacier surface in summer (snow or ice at 0 °C) efficiently cools the warmer air aloft and causes a density-driven downslope flow (referred to as a katabatic wind or glacier wind), which is most developed during periods of weak synoptic flow and strong insolation (e.g. Ohata, 1989; Van Den Broeke, 1997a, b; Greuell and Böhm, 1998; Oerlemans and Grisogono, 2002). The maximum wind speed of the low-level-katabatic jet is typically reached within a few metres above the glacier surface (Van Den Broeke, 1997b; Oerlemans, 2010; Mott et al., 2020; Nicholson and Stiperski, 2020), but the cooling effect of the katabatic wind layer while its cooling influence can extend up to 100m above the glacier surface m (Oerlemans and Vugts, 1993; Van Den Broeke, 1997a).

An upslope wind advecting warm and moist air from the valley usually forms develops during the day over above the cold and dry downglacier katabatic wind flow (Van Den Broeke, 1997b). The glacier wind is persistent during both day and nightkatabatic wind is generally persistent, but can be disturbed, especially near the glacier terminus, by a strong synoptic flow or a pronounced valley wind (Oerlemans and Grisogono, 2002; Mott et al., 2020; Nicholson and Stiperski, 2020; Shaw et al., 2024). Advection Such disturbances, and the associated advection of warm air from the periphery of a glacier during disturbance of the katabatic wind layer, together with glacier periphery and enhanced turbulent heat exchange, can locally and temporarily increase glacial glacier melt (Mott et al., 2020; Shaw et al., 2024). This means that More broadly, the response of the katabatic wind (i.e. its strengthening or weakening) near-surface circulations over glaciers to a warming environmentwill

have a direct impact on, whether through strengthening, weakening, or structural change, will directly impact the future energy and mass balance of mountain glaciers.

Assessing the impact of climate change on katabatic winds the structure of the boundary layer and the local circulation in glacierised mountain environments environments is difficult because multi-year long-term glacio-meteorological observations of downglacier katabatic winds and upglacier valley winds are very rare and only available from a few high elevation thermally driven winds in glacierised terrain remain scarce and are usually restricted to a handful of high-elevation sites. A recent comparative study focusing on three glaciers in the Swiss Alps has shown that the near-surface showed that the cooling effect of katabatic winds (from 1to -7 °C on warm afternoons) can vary varies widely between sites and depends, depending not only on glacier size. It also depends but also on the resistance of a glacier to the weakening of the katabatic wind layer and the the katabatic layer to intrusion of warm valley air, which is controlled inter alia by the in turn is strongly controlled by local topography and the orientation of the valley to the synoptic flow valley orientation (Shaw et al., 2024). Observations from the Himalaya suggest that the increasing difference between summer temperatures on and off glacier over the last three decades thermal contrast between glacier and non-glacier terrain has strengthened the katabatic wind and lowered the elevation of the convergence zone between cold-dry katabatic winds and warm-moist valley winds. This effect could explain both the observed flows, thereby cooling and drying of proglacial areas in this region (Salerno et al., 2023). However, the continued area loss of mountain proglacial areas (Salerno et al., 2023). Conversely, the ongoing shrinkage of glaciers will eventually lead to a decay of-weaken or even eliminate katabatic winds, as measurements from a retreating alpine glacier indicate (Shaw et al., 2023). The decay may be further enhanced by the increase in supraglacial debris cover, which promotes the disruption of katabatic winds-shown by recent measurements on retreating glaciers (Shaw et al., 2023), with debris cover further promoting disruption (Nicholson and Stiperski, 2020). In mountains that will-mountain valleys that are projected to become ice-free, climate model simulations suggest that warm air is likely to be advected further up the valley by local winds, as suggested by climate model simulations (Potter et al., 2018).

While meteorological measurements from automatic weather stations operated continuously or temporarily on mountain glaciers around the world have provided fundamental worldwide have provided valuable insights into near-surface winds, air temperature fields and turbulent temperature fields, and energy fluxes (e.g. Greuell and Böhm, 1998; Oerlemans and Grisogono, 2002; Shea and Moore, 2010; Petersen and Pellicciotti, 2011; Shaw et al., 2016; Steiner and Pellicciotti, 2016; Shaw et al., 2017; Mott et al., 2020; Nicholson and Stiperski, 2020; Shaw et al., 2021, 2023, 2024), techniques for atmospheric sounding to greater heights on mountain glaciers are still searce. Howeverto greater heights remain scarce. Yet, atmospheric soundings (i.e. vertical profiling of various atmospheric variables) are crucial for determining the vertical extent of the katabatic wind layer, for studying the resolving the vertical structure of the boundary layer, over glaciers and for investigating the interactions between the katabatic wind, other thermally driven local winds circulations (i.e. glacier, valley and slope winds), and the free atmosphere (i.e. synoptic flow) (e.g. Oerlemans, 2010). Meteorological instruments installed on a (e.g. Oerlemans, 2010). Traditional mast or tower measurements can extend the vertical measurement range, but the logistical effort is tremendous and the maximum height is usually limited to a couple of meters they are logistically demanding and limited to only a few metres above the glacier surface (e.g. Oerlemans and Vugts, 1993; Oerlemans et al., 1999; Litt et al., 2015).

Glacio-meteorological experiments with a large tethered balloon on Vatnajökull in Iceland (Oerlemans et al., 1999) and on Pasterze in the Austrian Alps (Van Den Broeke, 1997a, b; Oerlemans and Grisogono, 2002) allowed atmospheric enabled soundings up to several hundred metres above the glacier-surface already two decades ago. However, but to the authors' knowledge, since the comprehensive Pasterze experiment in the summer of 1994, no atmospheric 'knowledge, no comparable soundings have been carried out on any mountain glacier worldwide, presumably because of the logistical challenges and high costs involved. As a low-cost and lightweight alternative to tethered balloonsconducted on mountain glaciers since the Pasterze experiment in 1994, largely due to logistical and financial constraints. More recently, Unoccupied Aerial Vehicles (UAVs) equipped with meteorological sensors have increasingly been deployed in recent years for atmospheric boundary layer researchin the high latitudes, including have emerged as a promising, low-cost alternative for boundary-layer research, and have been successfully deployed in polar regions such as Antarctica, Greenland, and Iceland (e.g. Reuder et al., 2009; Cassano, 2014; Jonassen et al., 2015; Cassano et al., 2016; Lampert et al., 2020; Hansche et al., 2023). However, the feasibility and suitability of UAVs their feasibility for atmospheric sounding over alpine glaciers has not yet been demonstrated. Here, we describe

The aim of this study was therefore to develop a low-costand, open-source fixed-wing UAV for atmospheric boundary layer research on mountain glaciers, present the results of a feasibility study alpine glaciers and to evaluate its suitability for investigating glacier-atmosphere interactions and local circulations in complex terrain. To this end, we conducted two half-day (June and September) and two 24-hour (July and August) measurement campaigns on the Kanderfirn in the Swiss Alps in June 2021 under contrasting synoptic conditions. Here, we describe the developed measurement system and present the atmospheric data collected during the four campaigns, and discuss the benefits, challenges, and limitations of using meteorological UAVs in alpine terrainfixed-wing UAVs to study the structure of the boundary layer and local circulations in glacierised high mountain environments.

2 Study area

100

105

110

The Kanderfirn (46.47°N, 7.78°E), a south-west-facing valley glacier in the Swiss Alps (see Fig. 1), was chosen as selected as the test site for the UAV-based atmospheric soundings because the setting allowed to study the influence of the its setting is well suited to investigate how alpine terrain and the extensive snow cover on synoptic flow influence the occurrence of typical local winds circulations (i.e., katabatic, valley, and slope winds) and the structure of the atmospheric boundary layer over the glacier. Furthermore, there is already considerable experience of using UAVs a mountain glacier. In addition, considerable experience with UAV operations on this glacier from previous is available from previous field campaigns (Groos et al., 2019, 2022; Messmer and Groos, 2024). The glacier currently covers an area of approximately 12km km² and extends from 2300meter m above sea level (m a.s.l.) at the tongue to 3200m m a.s.l. in the accumulation area. To the north, the glacier it is bounded by the steep Blüemlisalp massif, with which reaches a maximum elevation of 3661 m a.s.l. (for a detailed description of the study area, see Groos et al., 2019).

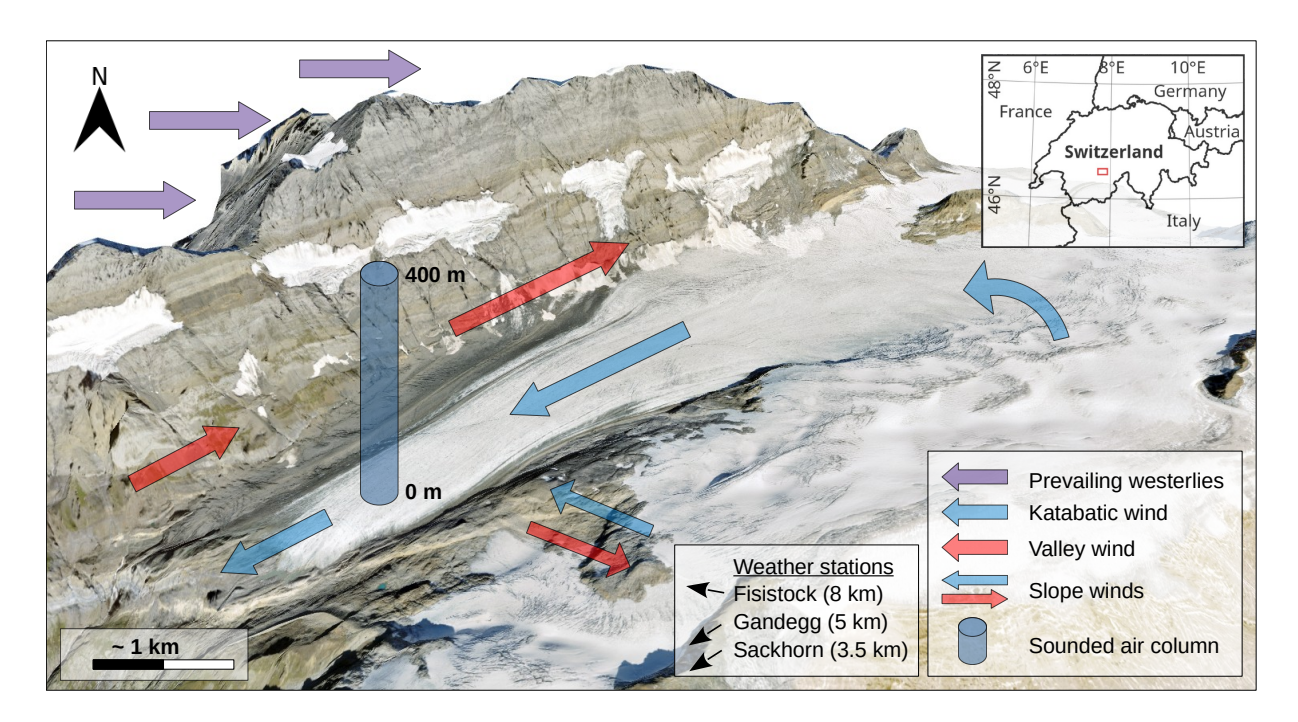


Figure 1. Overview of the alpine test site for the UAV-based atmospheric soundings and schematic of the synoptic flow and hypothesised dominant local winds on the Kanderfirn in the Swiss Alps. The approximate location of the nearby weather stations is indicated. The 3D model in the background is based on the SWISSIMAGE (orthophoto) and the swissALTI3D (digital surface model) from 2018, both provided by Swisstopo.

During the campaign on 16 June 2021, at the beginning of the melt season, the glacier was under the influence of a pronounced anticyclone over the Sahara (see Fig. 2) and surface was still fully snow-covered snow covered (see Fig. 4). The snow depth in the area of the atmospheric soundings was 4), with a snow depth of about 2 m in the sounding area. Snow-free conditions prevailed during the subsequent campaigns. Three automatic weather stations (see Fig. 1) operated by the WSL Institute for Snow and Avalanche Research (SLF), are located in the vicinity of the glacier: one at Fisistock (46.4715°N, 7.6739°E; 2160m- m a.s.l.), one at Gandegg (46.4293°N, 7.7606°E; 2720m- m a.s.l.), and one at Sackhorn (46.4397°N, 7.7662°E; 3200m- m a.s.l.), are located in the proximity of the glacier. These stations provide valuable supporting data for the broader interpretation of the atmospheric soundings.

3 Synoptic situation

135

On 16 June 2021, a pronounced ridge over central Europe (see Fig. 2a) created stable and warm conditions across the Bernese Alps (see Fig. 3). Subsidence maintained mostly clear skies and weak synoptic forcing, favouring the development of local valley circulations and thermally driven winds in the Kanderfirn area. During 9 to 10 July, on the contrary, the region was influenced by a cyclonic episode associated with a broad trough to the northwest of the Alps (see Fig. 1). Overview of the

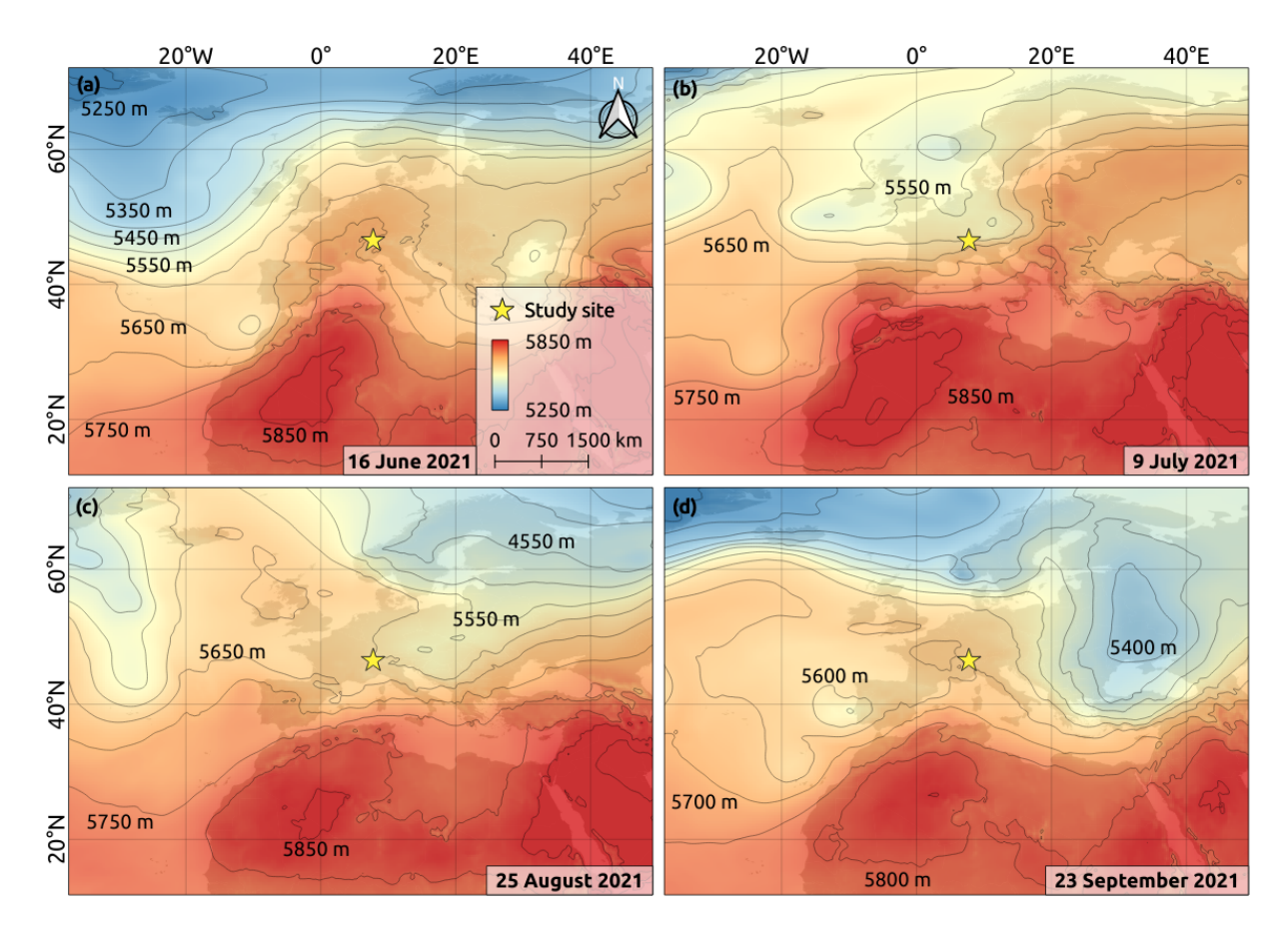


Figure 2. Synoptic situation at the time of the measurement eampaign (campaigns on 16 June (a), 9 July (b), 25 August (c) and 23 September 2021 (d). The synoptic weather ehart shows charts show the atmospheric thickness between the 1000 and 500 hPa pressure levels derived from ERA5 data. The study area was under the influence of an anticyclone over the Sahara. The diurnal cycle of air temperature

alpine test site for the UAV based atmospheric soundings and schematic of the synoptic flow and hypothesised dominant local winds on the Kanderfirn in the Swiss Alps. The approximate location of the nearby weather stations is indicated. The 3D model in the background is based on the SWISSIMAGE (orthophoto) and the swissALTI3D (digital surface model) from 2018, both provided by Swisstopo.2b). On the morning of 9 July, before the start of the campaign, rainfall persisted in the area, but following the passage of a cold front, warmer and drier air was advected towards the study site (see Fig. 3). At the end of August, the conditions on the northern side of the Alps were relatively cool and stable (see Figs. 2c and 3). On 25 to 26 August, shallow moist layers favored stratus formation, while the middle and upper troposphere remained dry and stable, limiting convective development. Finally, on 23 September, a strong anticyclone extended over central Europe (see Fig. 2d), producing clear, dry, and calm weather in the Bernese Alps. As in June, the absence of a significant synoptic forcing favoured the study of local and thermally driven winds on the glacier.

140

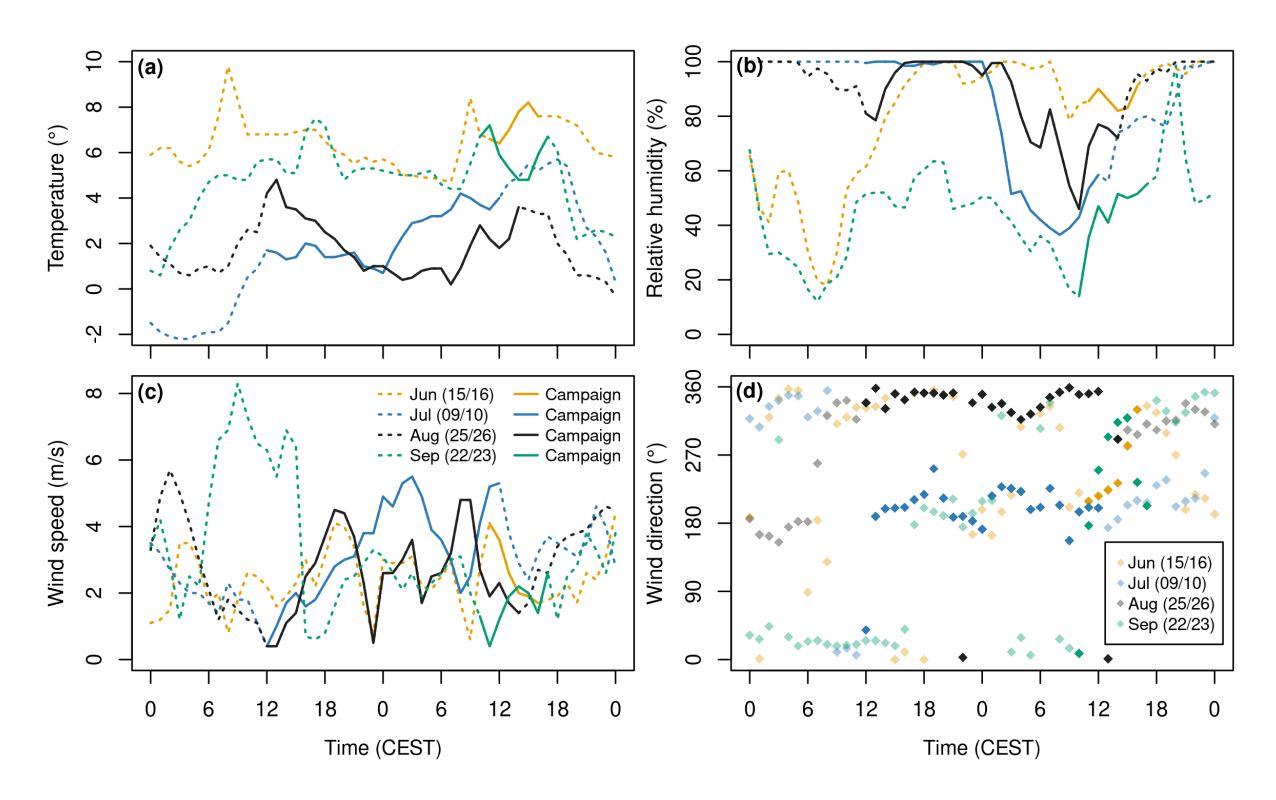


Figure 3. Temperature (a), relative humidity (b), wind speed (c), and wind direction on the day of (d) recorded at the UAV-based atmospheric soundings is shown for three-Sackhorn weather stations station in 2021 during two-day periods comprising the vicinity of the glacier (see Fig. 1) campaigns in June, July, August, and September.

4 Methodology

155

4.1 Unoccupied Aerial Systen

For the atmospheric sounding of the boundary layer over alpine glaciers, we designed a lightweight Unoccupied Aerial System (UAS) using low-cost and open-source software and hardware developed within the framework of the Paparazzi UAV project (Hattenberger et al., 2014). The UAS is very similar to the one presented by Groos et al. (2019) for photogrammetric surveys in alpine terrain and consists of a ground segment, an airborne segment (i.e. the UAV) and a communication segment. A mobile and lightweight ground control station (GCS) is necessary in the field for the configuration, monitoring and control of the UAV. Our GCS consists of a rugged outdoor laptop running the Paparazzi software, a remote control (Graupner HoTT mx-16 2.4 GHz) for manual operation of the UAV and a bi-directional wireless modem (XBee Pro S2B 2.4 GHz) for communication between the GCS and the UAV. The wireless modem supports both telemetry (downlink) and telecontrol (uplink).

The fixed-wing UAV for atmospheric sounding (see Fig. 24) was built from scratch and has a wingspan of 160 cm. We used expanded polypropylene (EPP) fuselage parts available from the aeromodelling community to build two identical flying wings. The centrepiece of the UAV is the open-source autopilot (Apogee v1.0) that supports automatic and autonomous flight

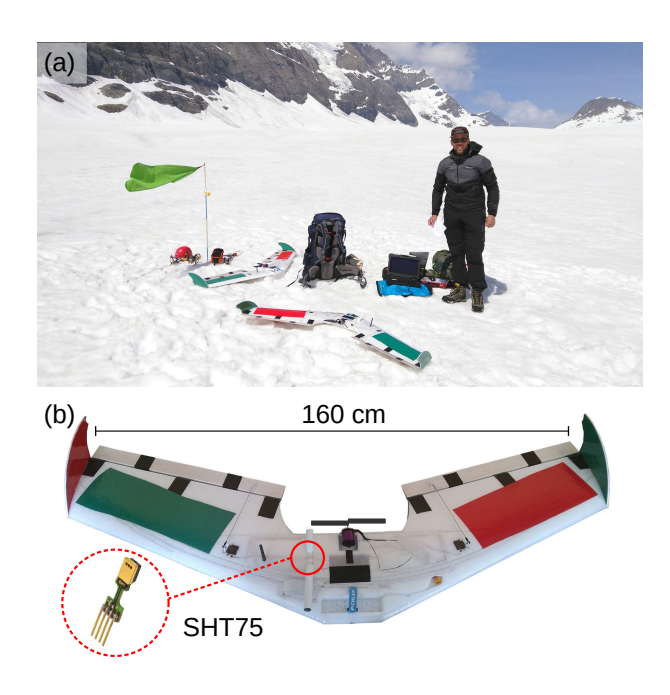


Figure 4. UAS and local conditions during the <u>first</u> measurement campaign -on 16 June 2021. (a) The Kanderfirn was completely snow-covered. The provisional weather vane (green flag) indicates the cold and dry katabatic wind that prevailed during the entire campaign. (b) Close-up view of the low-cost and open-source fixed-wing UAV equipped with a temperature and humidity probe (SHT75).

(Hattenberger et al., 2014). It was developed as part of the Paparazzi UAV project and can be replicated using the hardware design published online (https://wiki.paparazziuav.org/wiki/Apogee/v1.00). A rear-mounted brushless electric motor (Hacker A30-12XL V4) with carbon folding propellers in pusher configuration provides the necessary thrust. Two digital servomotors (KST DS145 MG) control the ailerons. For automatic flight and communication with the GCS and remote control, the UAV is equipped with a Global Navigation Satellite System (GNSS, Drotek U-blox NEO-M8T), a wireless modem (XBee Pro S2B 2.4 GHz) and a receiver (Graupner HoTT mx-16 2.4 GHz). A 5000 mAh lithium polymer battery powers the whole system and supports flight times up to 45 minutes. Several small lights on the UAV enable atmospheric sounding at night. A digital humidity and temperature sensor (Sensiron SHT75), with an accuracy of ± 1.8 % for relative humidity and of ± 0.3 °C for air temperature (Sensirion, 2024), is connected to the autopilot. The sensor is housed in a white tube to protect it from direct solar radiation (see Fig. 24). During the flight, air flows through the tube from the front to the back, ensuring adequate ventilation of the sensor. All collected data is stored on an SD card and syncronised using the clock of the autopilot. In total, the UAV weighs less than 2 kg and costs about 1200 EUR (excluding the GCS and remote control).

To cross-calibrate the temperature and humidity sensors on both UAVs (A2NO1 III and A2NO1 IV), a 24-hour intercomparison measurement was performed indoors from 4 to 5 June 2021 with an independent reference logger (see Fig. A1). A fan in front of the two UAVs and reference logger ensured adequate ventilation of the sensors. The mean difference in air temperature between both SHT75 sensors was 0.43 °C and the mean difference in relative humidity was 1.5 % (see Fig. A2).

4.2 Atmospheric soundings

180

185

190

195

200

205

The air column sounded by the fixed-wing UAV on 16 June 2024 was located in the central lower part of the glacier (46.46989°N, 7.777853°E, 2430m m a.s.l.), about 1 km from the terminus (see Fig. 1). A total of 8 40 flights, each (except one) consisting of two vertical profiles, were performed between 10 am and conducted during the four campaigns in 2021 (see Table 1). Two half-day campaigns were carried out on 16 June (8 flights) and 23 September (5 pm Central European Summer Time (CEST) (see Table 1 flights), and two 24-hour campaigns, including nocturnal soundings, on 9/10 July (14 flights) and 25/26 August (13 flights). Take-off (i.e., hand launch) and landing of the fixed-wing UAV on the glacier was performed manually were performed manually during the first three campaigns. For the last campaign, a bungee rope fixed into the glacier with an ice screw was successfully introduced to reduce the risk of failure during take-off. Planned take-offs on the hour had to be delayed at certain times of the day were occasionally delayed due to poor GPS accuracy (see Table 1).

For the vertical soundings, the UAV automatically followed a pre-programmed flight plan to measure air temperature and relative humidity up to 400m above the glacier surface m (see Fig. 5). To demonstrate the feasibility of extending soundings to greater heights, one flight at the end of the August campaign was conducted up to 800 m above ground level (m a.g.l.). After a rapid ascent, the UAV eircled at a pre-defined always circled for 60 s at the predefined maximum height (see Table1) for 60 seconds to give 1) to allow the SHT75 sensor enough time to adapt to the ambient air. The descent was performed in a spiral with constant throttle and a radius of 75 m to support the enable derivation of wind speed and wind-direction from the GNSS data (see Section 4.3). The sink rate was low A low mean sink rate on the order of 2 m s⁻¹ (see Fig. B1) was chosen to minimise the effect of sensor inertia (5 s for air temperature and 8 s for relative humidity to adapt to reach 63-% of a signal change). Once the UAV reached a height of descended to less than 10 mabove ground level (m a.g.l.), the sounding was repeated. A complete sounding (consisting of two vertical profiles) took about 10 to ascents and two descents) took approximately 15 minutes.

4.3 Data processing and analysis

The meteorological data (air temperature, relative humidity and air pressure) and flight recorder data (e.g. roll, pitch, yaw, battery voltage) collected during each sounding are stored in two different log files, which are synchronised using the clock of the autopilot. While the meteorological data are stored in a human readable text file, the flight recorder data are stored in a binary file that is decoded using checksums for further analysis. Decoding, post-processing and reformatting of the data is performed by the open-source FORTRAN software package mmp (mobile measurement post-processing) by Philipp (2024), which assigns all sensor messages to unified time steps and detects take-offs, touch-downs and outliers in the messages from the GNSS module. Time lag correction for the SHT75 sensor and calculation of horizontal wind components can also be performed by this package.

For the analysis of vertical and temporal variations of air temperature, humidity, wind speed, wind direction and turbulence over the glacier surface, only the data from the two consecutive descents (i.e. downward spirals) of each flight were considered, because the measurements from the two ascents are strongly affected by the rapid rate of climb (see Fig. 5)Figs. 5, 6). To account for sensor response times ($\tau = 5$ s for temperature, $\tau = 8$ s for humidity), we applied a time-lag correction to the

Table 1. Key figures of the UAV-based atmospheric soundings on 16 June, 9/10 July, 25/26 August and 23 September 2021.

Campaign date	UAV name	No. of Takeoff profiles time	Landing time	Max. height (m AGL)	Campaign date	UAV name	Takeoff time	Landing time	Max. height (m a.g.l.AGL)
2021-06-16	A2NO1 III	2 -10:41	10:51	250	2021-07-10	A2NO1 IV	10:03	10:19	400
2021-06-16	A2NO1 III	2- 11:10	11:22	350	2021-07-10	A2NO1 IV	12:00	12:15	<u>400</u>
2021-06-16	A2NO1 III	2 -12:00	12:12	350	2021-08-25	A2NO1 IV	2 -12:00	12:16	<u>400</u>
2021-06-16	A2NO1 IV	13:24	13:41	350	2021-08-25	A2NO1 IV	2 -14:00	14:15	<u>400</u>
2021-06-16	A2NO1 IV	14:01	14:17	350	2021-08-25	A2NO1 IV	16:00	16:15	<u>400</u>
2021-06-16	A2NO1 IV	2 -15:07	15:23	<u>400</u>	2021-08-25	A2NO1 III	20:44	20:59	<u>400</u>
2021-06-16	A2NO1 IV	16:00	16:15	<u>400</u>	2021-08-25	A2NO1 III	22:09	22:25	<u>400</u>
2021-06-16	A2NO1 IV	16:45	<u>17:00</u>	<u>400</u>	2021-08-26	A2NO1 III	00:04	00:18	<u>400</u>
2021-07-09	A2NO1 IV	12:09	12:25	<u>400</u>	2021-08-26	A2NO1 III	<u>02:</u> 07	02:22	<u>400</u>
2021-07-09	A2NO1 IV	13:00	13:15	<u>400</u>	2021-08-26	A2NO1 III	04:01	04:15	<u>400</u>
2021-07-09	A2NO1 IV	14:00	14:15	<u>400</u>	2021-08-26	A2NO1 III	06:14	06:18	<u>400</u>
2021-07-09	A2NO1 IV	15:00	15:14	<u>400</u>	2021-08-26	A2NO1 III	08:02	08:16	<u>400</u>
2021-07-09	A2NO1 IV	16:00	16:15	<u>400</u>	2021-08-26	A2NO1 III	10:09	<u>10:23</u>	400
2021-07-09	A2NO1 IV	2- 17:01	<u>17:</u> 16	<u>400</u>	2021-08-26	A2NO1 III	12:06	12:19	<u>400</u>
2021-07-09	A2NO1 IV	<u>18</u> :00	<u>18:</u> 16	<u>400</u>	2021-08-26	A2NO1 III	13:52	14:08	800
2021-07-09	A2NO1 IV	20:00	<u>20</u> :15	400	2021-09-23	A2NO1 III	10:10	10:24	<u>400</u>
2021-07-10	A2NO1 IV	2 -23:56	00:13	<u>400</u>	2021-09-23	A2NO1 III	12:21	12:36	<u>400</u>
2021-07-10	A2NO1 IV	02:00	02:16	<u>400</u>	2021-09-23	A2NO1 III	14:01	14:14	<u>400</u>
2021-07-10	A2NO1 IV	04:01	04:17	<u>400</u>	2021-09-23	A2NO1 III	<u>16:01</u>	16: 45 - <u>16</u>	400
2021-07-10	A2NO1 IV	05:59	<u>06:15</u>	<u>400</u>	2021-09-23	A2NO1 III	17: 00-47	<u>18:01</u>	400

descent profiles, followed by a Gaussian low-pass filter (σ = 1/3 s) to limit noise amplification. The first descent of each sounding lacks data from the lowest metres above the surface, as the uneven terrain and GPS accuracy did not support flying below 10m a.g.l. m AGL before the start of the second climb. The second descent covers the full profile down to the surface. Due to the limited GPS accuracy, the recorded absolute flight altitude varied by a few metres between the different soundings. Therefore, we used the average altitude before take-off and after landing of each flight to standardise the base height of all soundings.

215 For each individual vertical profileon 16 June 2021, air temperature was aggregated into 1 from both descents was merged and binned into 5 m height intervals for consistent comparisonof the different soundings by applying a central moving average with a sampling window of 5 m (2 m above and 2 m below each 1 m layer) to the original measurements. The air temperature measured by UAV A2NO1 III during the first three soundings (see Table 1) was adjusted to harmonise the SHT75 sensors of both UAVs (A2NO1 III and A2NO1 IV) using a correction factor of 0.43 °C obtained from the 24-hour intercomparison

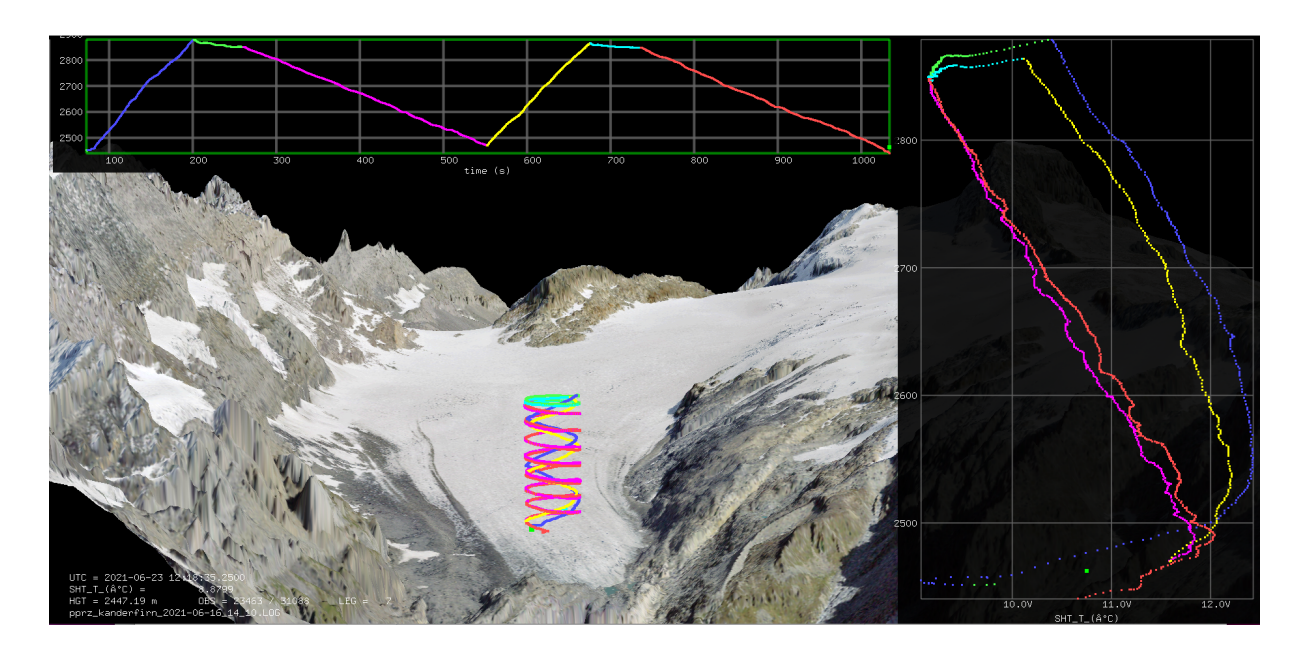


Figure 5. Screenshot of the graphical user interface of the open-source software package mmp for data post-processing and 3D visualisation. The top panel shows the flight altitude (m) over time, the middle panel shows the flight path of two subsequent soundings and the right panel shows the temperature profiles for two climbs and two descents at about 13:30 CEST. Note that the air temperature measured during the two rapid climbs has a warm-bias due to the inertia of the sensors.

measurement (see Appendix A). To estimate the thickness of the cool katabatic wind that prevailed throughout the campaign was predominant during all campaigns, we calculated the top height of the surface-based inversion (SBI) visible in all-most air temperature profiles as follows. We considered air temperature (T) as a function of altitude (z):

$$T = T(z) \tag{1}$$

To eliminate the short-term variability superimposed on the general air temperature change with altitude, we applied a low-pass

filter (local polynomial regression) to smoothed the air temperature measurements from the second descent, which went

(extending down to the glacier surface) using a Savitzky-Golay filter (Savitzky and Golay, 1964). This filter applies a local

polynomial fit within a moving window, which preserves the overall structure of the vertical profile while reducing high-frequency

noise. We then computed the first derivative of the smoothed air temperature profile with respect to altitudebecause the top

height, since the top of the SBI is characterised by a transition of the temperature ehange rate gradient from positive to

negative values : (see Fig. C1b).

$$T'(z) = \frac{dT}{dz} \tag{2}$$

The lowest altitude $(z = z_i)$ where the first derivative is zero was determined as the top height (z_i) of the SBI:

$$z_i = \min\{z \mid T'(z) = 0\} \tag{3}$$

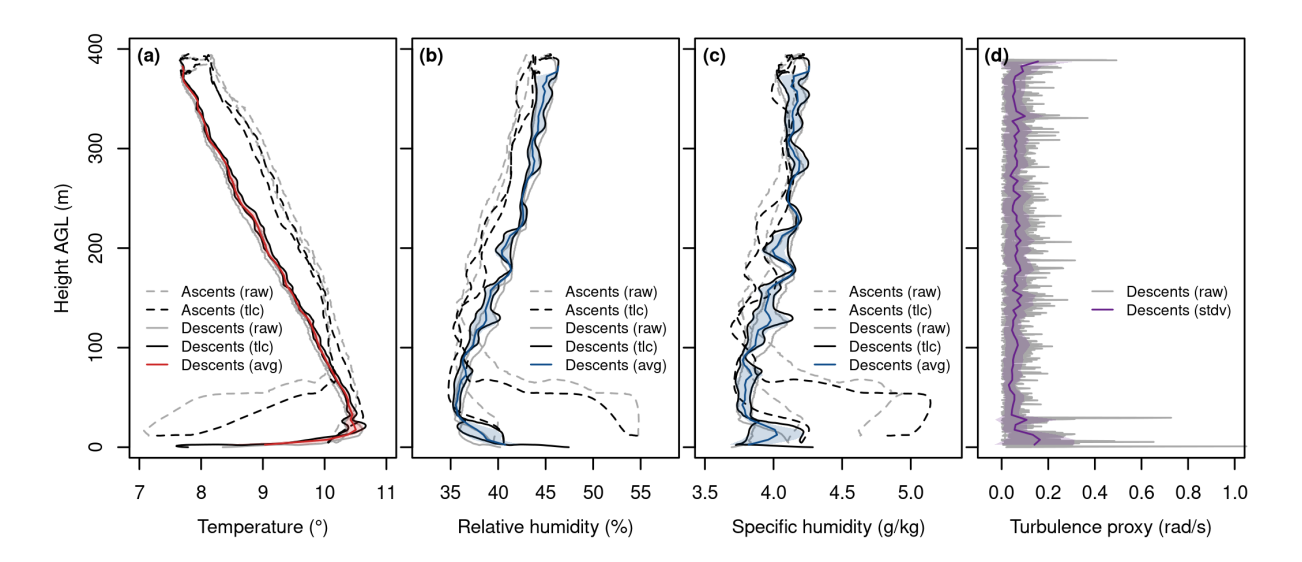


Figure 6. Example profiles of measured air temperature (a), measured relative humidity (b), derived specific humidity (c), and estimated turbulence (d) from the sounding on 23 September 2021 at 14:00 CEST, based on both ascent and descent data. raw = measurements recorded on the SD card, tlc = time-lag-corrected, avg = average profile from both descents. Shaded areas denote the standard deviation between the two profiles.

To calculate the lapse rate (i.e. air temperature gradient) above and below the top height of the SBI (z_i) , we performed a simple linear regression (see Appendix $\ref{eq:condition}$). For the data points below z_i , the linear regression model can be expressed as:

$$T(z) = a_1 z + b_1 \quad \text{for} \quad z \le z_i, \tag{4}$$

where a_1 is the lapse rate below z_i and b_1 is the intercept. For the data points below above z_i , the linear regression model can be expressed as:

$$T(z) = a_2 z + b_2 \quad \text{for} \quad z \ge z_i, \tag{5}$$

240 where a_2 is the lapse rate above z_i and b_2 is the intercept. In addition to the UAV-based lapse rates, we also calculated the environmental lapse rate for the study area at the time of each sounding using data from three nearby weather stations: Fisistock, Gandegg and Sackhorn (see Appendix ??Figs. 1, C1).

Since spatio-temporal variations in relative humidity (RH) can be the result of changes in air temperature, air pressure and/or water vapour, it is not an unambiguous parameter for analysing and interpreting changes in air moisture. Specific humidity (q) is more suitable as it is not sensitive to air temperature or pressure. We have therefore converted the recorded relative humidity (%) into specific humidity (g/kg) as follows (see Fig. 6):

The partial vapour pressure at saturation (p_s) for a given air temperature (T) is calculated using empirical constants from DWD (1976) by:

$$p_s(T) = E_0\left(\frac{A \cdot T}{B + T}\right),\tag{6}$$

where $E_0 = 6.10780$ hPa, A = 17.08085 and B = 234.175 K. The actual vapour pressure (e) is then given by:

$$e = p_s \frac{RH}{100},\tag{7}$$

Finally, the specific humidity (q) in g per kg is calculated as:

$$q = \frac{m_v}{m_a} \left(\frac{e}{p - 0.377e}\right) 1000,\tag{8}$$

where m_v is the molar mass of water vapour (18.01534 g/mol), m_a is the molar mass of dry air (28.9644 g/mol) and p is the pressure (in hPa) either measured or calculated from elevation assuming the standard atmosphere. As with air temperature, specific humidity was then resampled at 1the specific humidity data from both descents were merged and binned into 5 m height intervals using a central moving average to ensure consistent comparison of the different to allow consistent comparison across soundings.

Unlike air temperature and humidity, wind speed, wind direction and turbulence were not measured directly. These three parameters had to be derived from the GNSS data and the recordings made by the inertial measurement unit. The wind estimation algorithm is based on the concept described by Mayer et al. (2012) and Bonin et al. (2013). The wind direction is estimated from the variation in ground speed during a full circle of the flight path with all UAV flight controls, in particular throttle and pitch, held constant. The (opposite) wind direction is then the flight direction at maximum (minimum) ground speed within a circle. The wind speed can be assumed to be the difference between the average ground speed during a circle and the maximum or minimum ground speed.

As a rough approximation of turbulence, the roll rate recorded by the inertial measurement unit at 4 Hz can be used, since eddies with diameters ranging from a few decimetres to a few metres, acting differently on the two wings, cause short rotational movements around the longitudinal axis of the UAV. Intensity The intensity of turbulence can then be estimated by calculating the standard deviation of the roll rates within a certain vertical section. In order to focus on the vertical scale of several meters, the turbulence proxy is calculated for 15 m height intervals by applying a central moving standard deviation with a sampling window of 10 m to the recorded roll rate computing the standard deviation of all roll rate data points from both descents that fall into the respective bin. This proxy measure of turbulence can only be a rough estimate, as large parts of the turbulence spectrum are missing. Therefore absolute values, absolute values, e.g., for turbulence kinetic energy (TKE) can not, cannot be derived. However, it is able to depict the general tendency of relatively increasing or decreasing turbulence. Details on this method are published in a separate paper.

5 Results

255

260

265

The atmospheric boundary layer above the glacier tongue of Kanderfirn warmed steadily from late morning (10:45) to late afternoon (16:05) on 16 June-

5.1 General boundary layer structure and local circulations

The 40 profiles of air temperature, specific humidity, wind speed, and wind direction obtained from UAV-based atmospheric soundings during four measurement campaigns on the Kanderfirn in summer 2021, with a particularly strong warming around noon (12:05) (see Fig.??). Interestingly, none of clearly reflect the prevailing synoptic situation, while also revealing characteristic patterns of boundary layer structure and local circulations in alpine terrain. An overview of all profiles from each campaign is provided in Fig. 7.

285

290

295

300

305

310

The two consecutive descent measurements of temperature and humidity from each flight agree closely, as indicated by the narrow shaded area around the three nearby weather stations recorded any particular warming around midday, which could indicate the advection of warm air (see Fig.2). During the last sounding of the campaign in the late afternoon (16:45), a cooling of the whole air column from the glacier surface up to 400 m amean profiles in Fig. 7. This consistency supports the reliability and representativeness of the individual soundings. Larger deviations (e.g.l. had already started. While the maximum air temperatures during each sounding were reached a few tens of meter above the ground, minimum air temperatures were recorded close to the glacier surface (see Fig. ??).

Course of the air temperature over the tongue of the Kanderfirn on 16 June 2021 derived from the second descent of each UAV flight.

In addition to the general course of air temperature over the glacier surface, which is well visible in the heat map > 0.5 °C, > 0.5 g/kg) between successive descents at certain height levels (see for example the 10:20 flight in September, Fig. 7d) suggest short-term dynamics and local mixing within the glacier boundary layer, but such cases are overall rare. In contrast, wind speed and wind direction profiles from a given flight naturally show higher temporal variability, yet they still generally match well (Fig. ??), the air temperature profiles up to 400 m a.g 7). I. derived from the two consecutive UAV descents of each sounding show characteristic variations in the vertical structure of the atmospheric

The aggregated mean profiles for each campaign highlight substantial variability between synoptic conditions: mean air temperature differed by up to 6 °C and specific humidity by up to 4 g/kg (Fig. 8), underscoring the strong influence of large-scale weather patterns on the glacier boundary layer (Fig.??). The two profiles from each sounding are more or less consistent (apart from deviations in the lowest metres of the 16:05 profiles), which gives confidence in the reliability and representativeness of the individual soundings. A surface-based inversion (SBI), most developed in the afternoon hours, can be seen in every second descent profile (reaching the ground) and in most first descent profiles (reaching about 10 m a.g.l.). The top height of the SBI varied between 10 and 50 m a .g.l. during the campaign 2). By contrast, the aggregated mean wind speed and wind direction profiles are strikingly similar across all campaigns, despite large variability within each campaign. All four exhibit a characteristic C-shape: relatively high wind speeds (4–5 m/s) near the glacier surface, a decrease with height up to about 100 m AGL, low wind speeds (about 2 m/s) between 100 and 200 m AGL, and a subsequent increase up to 400 m (Fig.??a). There was a marked increase in air temperature from the glacier surface to the top of the SBI. The warming rate (equivalent to a negative lapse rate) from 8). Notably, the wind speed decrease in the lower part coincides with a shift in mean wind direction from east-northeast (70-90°, down-glacier) to southwest (220-240°, up-glacier).

A distinct surface-based inversion (SBI) characterises all aggregated mean temperature profiles, especially in June and September (Figs. 8, 9). The SBI is characterised by a sharp temperature increase and, in some cases, also by a marked increase

in Moisture above the glacier surfaceto the top of the SBI ranged from 0.02 °C per 10 m (at. With the exception of five soundings in July and four in August, a SBI was present in all profiles. Across campaigns, the mean SBI top height is 38 ± 12:05) to 1.8 °C per 10 m(at 15:15) and had a mean value of 0.5m. The mean lapse rate below the SBI is -0.31 ± 0.21 °C per 10 m(Fig. ??c). Above the SBI, the air temperature decreased linearly up to the maximum height of the sounded air column. The whereas the mean lapse rate above the SBI increased from 0.4(or above the glacier surface in its absence) is 0.68 ± 0.13 °C per 100 min the late morning to about 0.8. This latter value closely matches the mean environmental lapse rate (0.66 ± 0.13 °C per 100 mafter noon (Fig. ??b), due to the stronger warming rate of the lower part of the boundary layer above the SBI (Figs.?? and ??). Compared to the UAV-derived lapse rates,) derived from the three nearby weather stations at the times of the soundings (Fig. 1). However, larger deviations between the lapse rate above the SBI or glacier surface and the environmental lapse rates calculated from the data of the three nearby weather stations show almost no temporal variability and are slightly higher on average (0.78 vs. 0.71 °C per 100 m). Overall, the air temperature change rate below the top height of the SBI is 15 times greater than above environmental lapse rate are evident at the time of individual soundings.

Course of the specific humidity (SH) over the tongue of the Kanderfirn

5.2 Boundary layer evolution (16 June 2021)

330

335

340

345

The half-day campaign on 16 June 2021 derived from the second descent of each UAV flight.

Similar to the air temperature, the water vapour in the sounded air column above the glacier tongue increased steadily during the campaign, from about 7.5 g kg⁻¹ (vertical mean) in the 2021 (late morning to about 8.5 g kg⁻¹ (vertical mean) in the late afternoon (see Fig. ?? late afternoon, 8 soundings) took place under the influence of an anticyclone over the Sahara, which created overall stable conditions in the study region (see Section 3 and Fig. 2). The heat map clearly shows that the cool air below the top height of the SBI is significantly drier than the air above. For example, in the late afternoon (at 16:05 and 16:45), specific humidity increased from less than 6.5 g kg⁻¹ near the glacier surface to almost 8.5 g kg⁻¹ at less than 50 m height. Apart from this, water vapour generally varied much less with altitude than air temperature June campaign was characterised by the warmest and most humid air column of all four measurement periods (Fig. 8). A distinct SBI was observed throughout the campaign, consistently present in all soundings and representing a defining feature of the boundary layer structure over the glacier during this period (Fig. 7a).

The mean top height of the SBI was relatively high at 47 ± 12 m (Fig.??).

Humidity profiles over the tongue of the Kanderfirn on 16 June 2021. Note that only the measurements from the two consecutive UAV descents (not from the ascents) are shown here.

In contrast to air temperature and water vapour, wind speed did not increase during the campaign and was highly variable vertically and temporally. Within individual profiles, wind speed varied from less than 1 m s⁻¹ to a maximum of 8 ms⁻¹ 9a). Below the SBI, a distinct negative lapse rate of -0.46 °C per 10 m was observed, indicating a sharp temperature increase just above the glacier surface. Above the SBI, the mean lapse rate was 0.72 °C per 100 m. From late morning to afternoon, the lapse rate above the SBI gradually increased, while the near-surface inversion remained pronounced (Fig. ?? 9b,c). The wind speed profiles from the two consecutive descents of each flight are in relatively good agreement, but also show short-term deviations

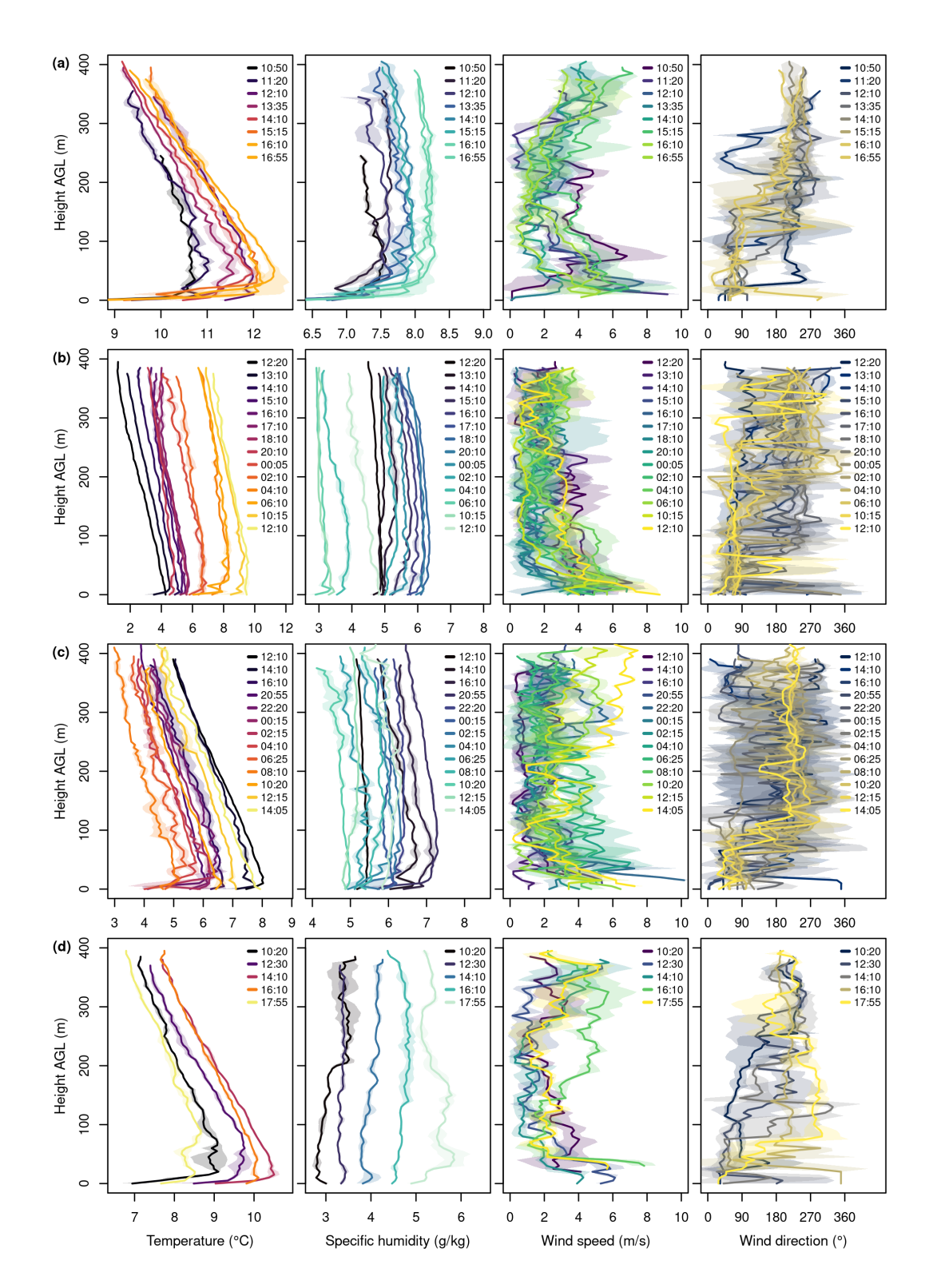


Figure 7. Air temperature Overview of all 40 profiles over the tongue of air temperature (first column), specific humidity (second column), wind speed (third column), and wind direction (fourth column) from the Kanderfirm measurement campaigns on 16 June 2021. Note that only the measurements from (a), 9/10 July (b), 25/26 August (c), and 23 September 2021 (d). Shaded areas indicate the two standard deviation between consecutive UAV descents (not from the ascents) are shown hereof each sounding.

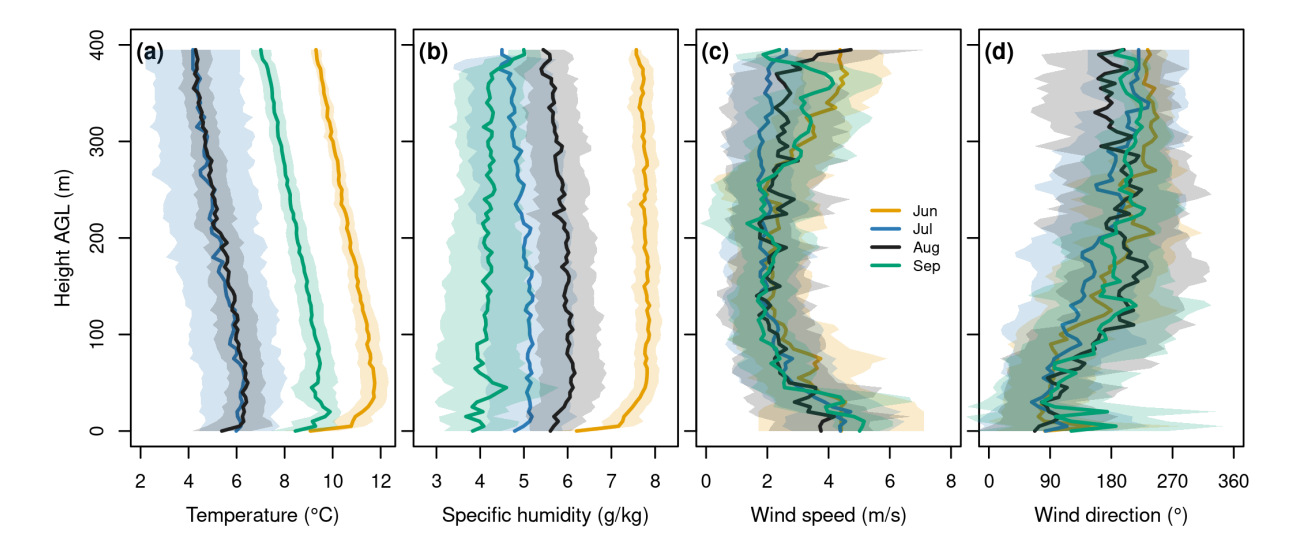


Figure 8. Course of the structure of the atmospheric boundary layer over the tongue Mean profiles of the Kanderfirn on 16 June 2021. air temperature (a), specific humidity (b), wind speed (c), and wind direction (d) for all four campaigns (summarised from Fig. 7). Shaded areas indicate the standard deviation across all profiles within each campaign.

at similar altitudes katabatic wind coincided with exceptionally dry conditions near the surface, more distinct than during any other campaign, as illustrated by the synthesis plot from the 16:55 flight (Fig. ??). Apart from the soundings at 10:45 and 13:30, a clear pattern is visible in all profiles that reached the ground: 10a,b).

350

355

360

365

Wind profiles exhibited the typical C-shape found across campaigns, with relatively high wind speeds up to 8 m s-1 were observed close to the glacier surface. From the glacier surface to about 100-200 m a.g.l. the at the surface, a decrease with height, and a subsequent increase (Fig. 7a). In the 16:55 example profile, wind speed decreased to 0-2 ms⁻¹. Above the calm layer, the wind speed increased again, reaching values of 3-6 m s⁻¹ at about 400 m a.g.l. from the surface up to about 170 m, where wind direction shifted abruptly from 80–90° (glacier wind) to 240–250° (valley wind) (Fig.??). The mean wind speed (about 2-4 m s⁻¹) measured at the three nearby weather stations during the campaign (Fig.2) was much lower than the wind speed observed near- 10c,d).

The temporal evolution of the boundary layer is captured by the heat maps of air temperature, specific humidity, and turbulence (Figs. 11–13). A continuous warming of the entire column was observed until around 16:10, after which cooling set in (Figs. 7a, 11a). Specific humidity increased steadily throughout the afternoon (Figs. 7a, 12a). No clear diurnal trend in turbulence was detected, although enhanced turbulence was present in the lowest 20–30 m above the glacier surface (ef. Fig.??Fig. 13a).

The dominant wind direction in the lowest 100-150 m of the sounded atmospheric boundary layer above the glacier surface was northeast (about 55°; see Fig.??), similar to the orientation of the lower part of the glacier and the assumed direction of the glacier wind (cf. Fig. 1). In contrast, the main wind direction above 250 m a.g.l. was southwest (about 235°; see Fig. ??),

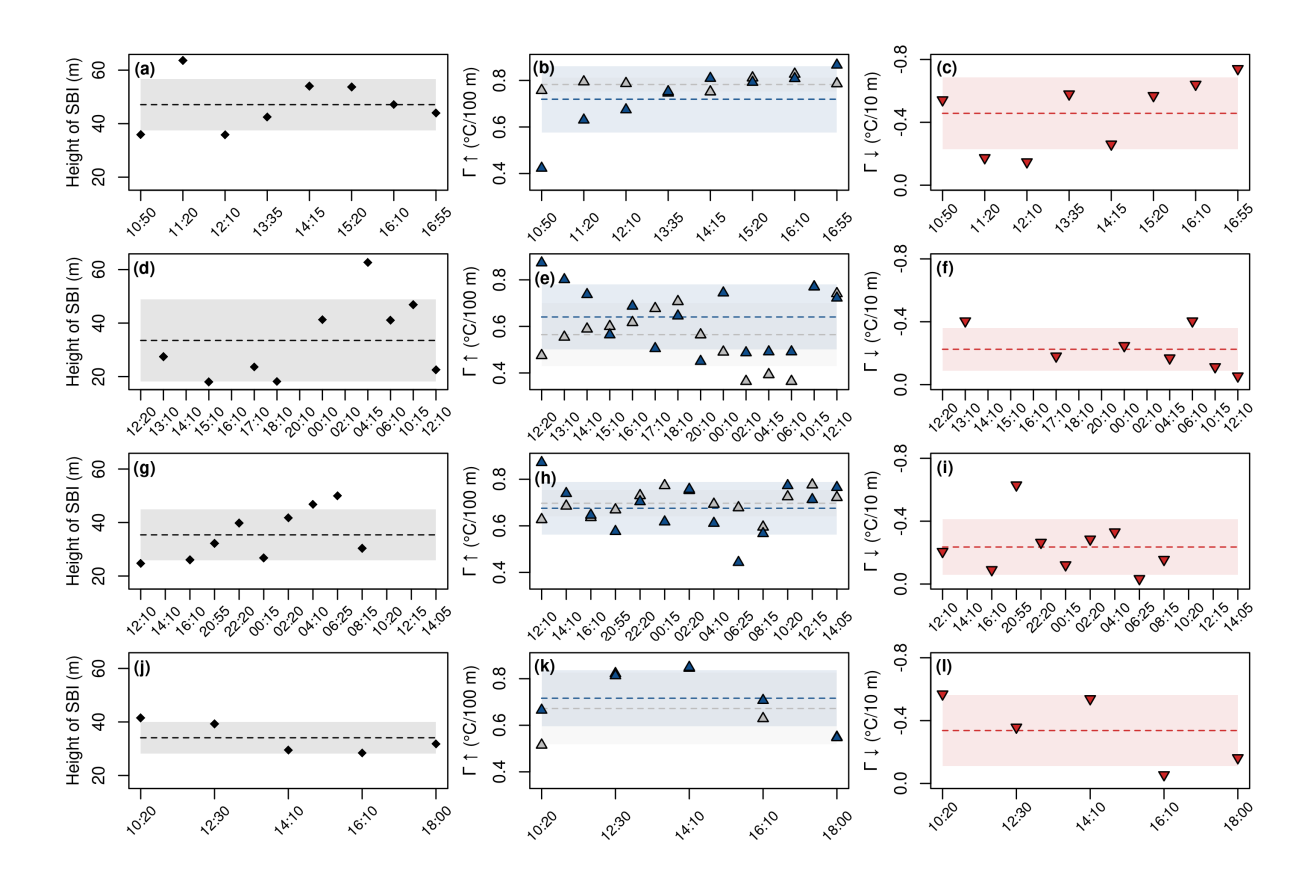


Figure 9. Top height of the surface-based inversion -(bSBI; first column) Lapse, lapse rate above the surface-based inversions SBI (SBIs \(\Gamma\)) in °C per 100 m derived from or above the glacier surface when no SBI was present together with the UAV soundings and environmental lapse rate in the area of the glacier calculated from data of three the nearby weather stations (Fisistock, Gandegg, and Sackhorn). (esecond column) Lapse, and lapse rate below the SBIs in °C per 10 mSBI (\(\Gamma\), third column) for each profile of the June (a-c), July (d-f), August (g-i), and September (j-l) campaigns. Dashed lines show indicate the campaign mean, and shaded areas represent the standard deviation.

similar to the orientation of the ice-free valley below the glacier terminus and the assumed direction of the valley wind (cf. Fig.1). The layer of strong wind shear of the order of 180° (from northeast to southwest) varied between the soundings from about 50-150 m a.g.l. (e.g. at 16:05; see Fig.??) to 150-250 m a.g.l.

370 5.3 Boundary layer evolution (9/10 July 2021)

375

The first 24-hour campaign on 9/10 July 2021 (e.g. at 12:05; see Fig.??) and corresponded well with the layer of reduced wind speed (cf. Fig.??). A clear difference in wind direction can also be seen in the data from the three nearby weather stations. While the two upper stations at 2720 and 3200 m a 14 soundings) was influenced by a cold front passage just before the start of measurements, leading to mainly southwesterly synoptic flow during the campaign, as indicated by the Sackhorn weather station (see Section 3 and Figs. 2, 3). Compared to June, the surface-based inversion (SBI) was less pronounced during July.

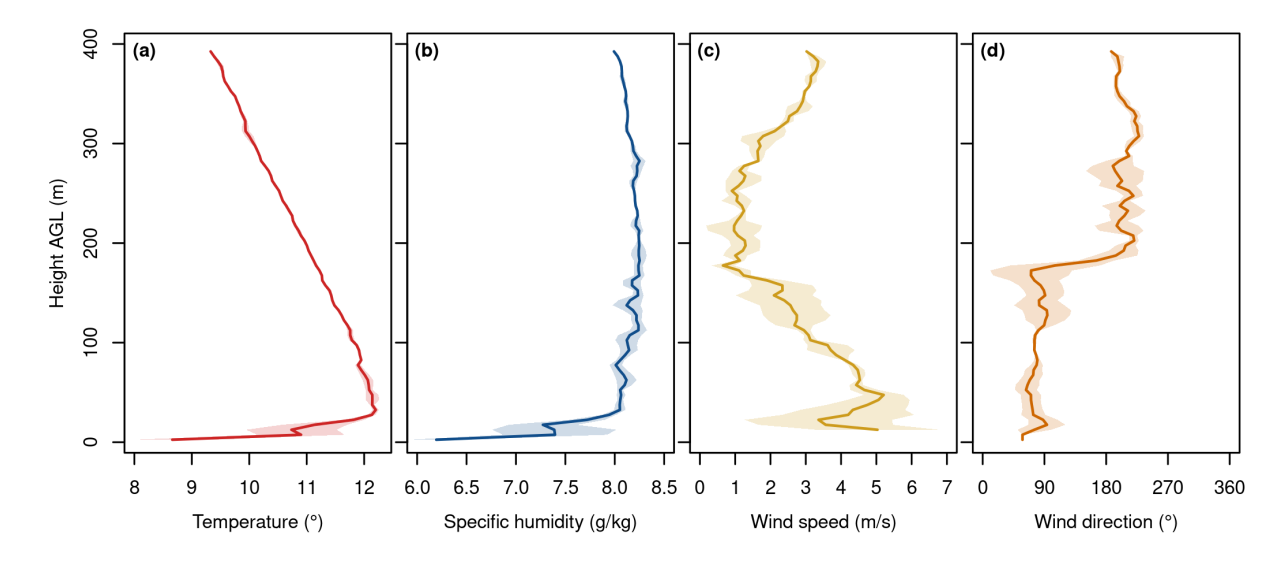


Figure 10. Course of the Synthesis plot showing air temperature (a), specific humidity (b), wind speed (***c*) over the tongue of and wind direction (d) profiles from the Kanderfirm 16:55 sounding on 16 June 2021 derived from the second descent of each UAV flight. 2021.

An SBI was absent in five soundings (Fig. 9d), and the mean SBI top height was relatively low at 34 m. s.l. recorded a mean wind direction of 290° and 255° (west) on 16 June 2021, the lower station at 2160 m a.s.l. at the end of the valley below the Kanderfirn recorded a mean wind direction of The mean lapse rate above the SBI was 0.64 °C per 100° (east), pointing towards the glacier terminus (m, representing a moist adiabatic profile, while the lapse rate below the SBI was stronger at -0.22 °C per 10 m. During the night, lapse rates above the SBI differed from those derived from nearby AWS observations, showing reverse profiles, but became more homogeneous after midnight (Fig. 2) 9e).

380

385

390

The boundary layer evolution over the campaign showed continuous warming from the first sounding at midday on 9 July until the last sounding at midday on 10 July, with warming persisting even during the night (Fig. 11b). A striking feature was the advection of warm and dry air after midnight (Figs. 11b, 12b), which coincided with periods of relatively strong turbulence throughout the entire sounded air column (Fig. 13b).

Wind speed profiles over the tongue of the Kanderfirn on 16 June 2021. Note that only the measurements from the two consecutive UAV descents (not from the ascents) are shown here. Wind profiles during this campaign generally exhibited the typical C-shape seen across other campaigns. Despite weaker inversions, the overall boundary layer structure was still influenced by local circulations, with katabatic flow dominating close to the glacier surface. The combination of weaker near-surface inversion, continued warming, and warm, dry advection resulted in a more mixed boundary layer than during the strongly stable June campaign.

The simple turbulence proxy derived from the UAV roll rate (the standard deviation at 10 m height intervals) revealed short-term

Wind direction at different heights above the tongue of the Kanderfirn on 16 June 2021 derived from the second descent of each UAV flight.

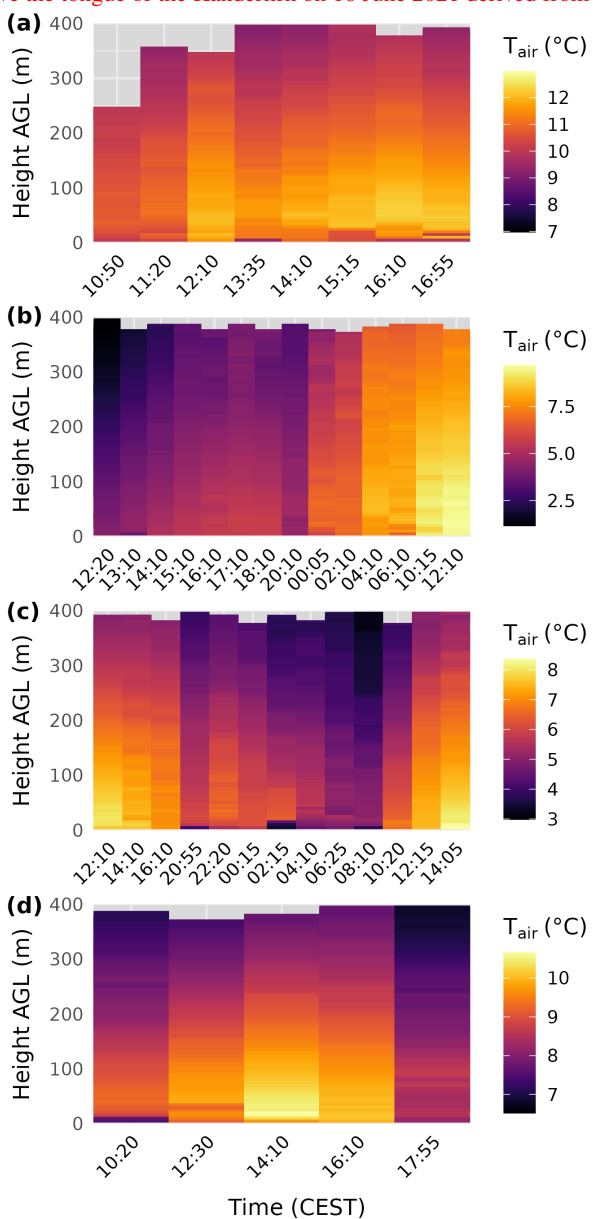


Figure 11. Heat maps of the temporal evolution of air temperature over the tongue of the Kanderfirn during the four measurement campaigns in 2021: 16 June (a), 9/10 July (b), 25/26 August (c), and 23 September (d). Note that the temperature scale differs between campaigns.

5.4 Boundary layer evolution (25/26 August 2021)

The second 24-hour campaign on 25/26 August 2021 (13 soundings) was characterised by relatively cool, moist, and stable conditions (see Section 3 and Fig. 2). As in July, glacier wind and small-scale variations in turbulence over the glacier during the campaign a surface-based inversion (SBI) were present throughout most of the campaign (Fig. 7c). An SBI was detected in all profiles except four, with a mean top height of 35 m. The mean lapse rate above the SBI was 0.67 °C per 100 m, consistent with a moist adiabatic profile, while the mean lapse rate below the SBI was -0.24 °C per 10 m. Lapse rates above the SBI showed relatively good agreement with the calculated environmental lapse rates (Fig.??). In general, turbulence was most pronounced in the lower 30 m of the atmospheric boundary layer. Increased turbulence was also observed in the layer of wind shear and decreased wind speed 9h). For example, during the last sounding (16)

The boundary layer exhibited characteristic diurnal variations. Temperature decreased from the first midday sounding on 25 August, reaching maximum cooling by the morning of 26 August, with the largest cooling at 400 m observed around 10:50), wind speed decreased from the glacier surface to about 200 m a .g.l. (Fig. ??) and wind shear (from northeast to southwest) occurred between about 100 and 250 m a.g.l. 00. Warming began in the lower part of the profile thereafter and continued until the end of the campaign in the early afternoon of 26 August (Fig. ??) 11c). Specific humidity increased from the start of the campaign until the evening (21:00) and then decreased until midday on 26 August (Fig. 12c).

Relatively strong turbulence was observed throughout the day, coinciding with substantial variations in wind speed between individual soundings (Figs. 3, 7c, 13c). The combination of a persistent SBI, cool and moist conditions, and variable wind speeds resulted in a moderately mixed boundary layer with pronounced diurnal thermal variations.

5.5 Boundary layer evolution (23 September 2021)

405

410

425

The final half-day campaign on 23 September 2021 (midday to midday, 5 soundings) took place under a strong anticyclone extending over central Europe, producing relatively warm and dry air, stable conditions, and weak synoptic flow (see Section 3 and Figs. 2, 3). A pronounced surface-based inversion (SBI) was present throughout the campaign (Fig. Exactly in this layer the turbulence was increased compared to the air layer below (30-100 m a.g.l. 7), with a mean top height of 34 m. The mean lapse rate above the SBI and glacier surface was 0.71 °C per 100 m, similar to June, and showed the best agreement with environmental lapse rates among all four campaigns (Fig. 9k). Below the SBI, the lapse rate was stronger than in July and August, at -0.34 °C per 10 m, reflecting the development of a pronounced katabatic wind near the glacier surface (Fig. 9l)and above (250-400 m a. g.l.). Consequently, during the sounding at 13:30, when no clear wind shear and no distinct wind speed change was observed, no increased turbulence could be detected (except from the lowest 20 m)

The boundary layer evolved with warming from the start of the campaign in the morning until approximately 14:00, followed by cooling until the end of the campaign (Fig. 11d), an earlier onset than observed in June and August. Specific humidity increased steadily throughout the campaign (Fig. 12d). Turbulence was stronger around midday and in the lower part of the profiles, with minimum turbulence observed in the upper part of the profiles during late morning and late afternoon (Fig. ??) 13d), indicating stable conditions and suppressed vertical mixing.

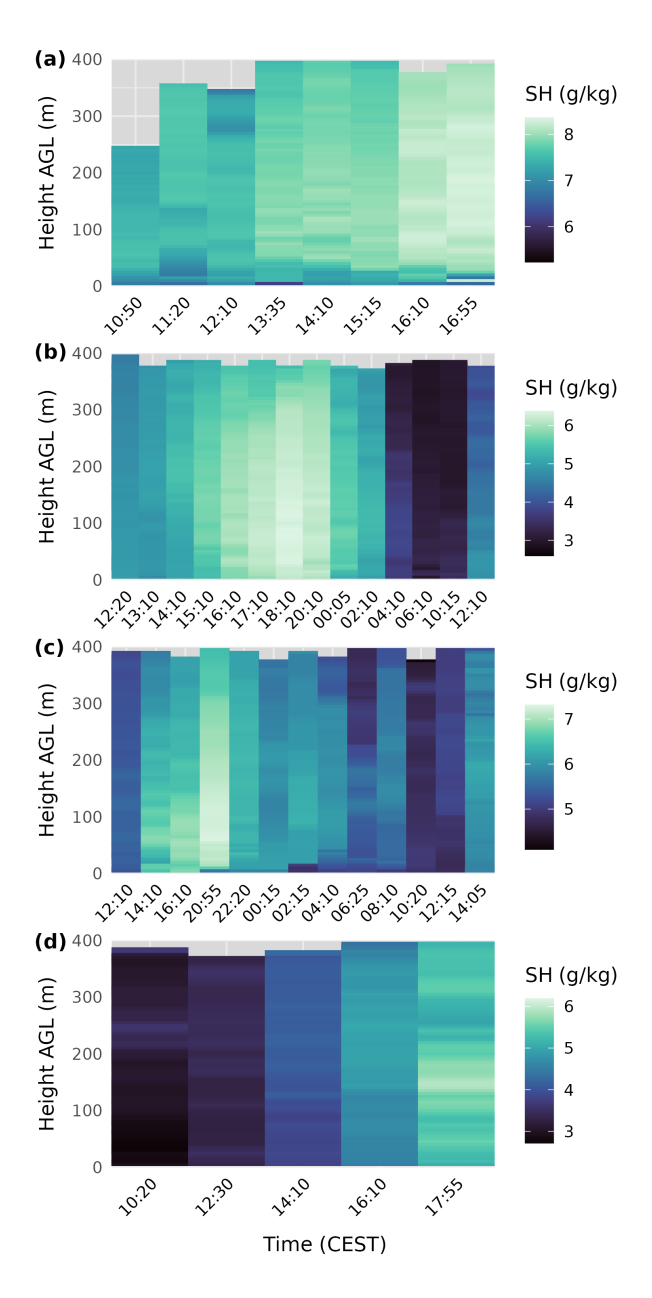


Figure 12. Heat maps of the temporal evolution of specific humidity over the tongue of the Kanderfirn during the four measurement campaigns in 2021: 16 June (a), 9/10 July (b), 25/26 August (c), and 23 September (d). Note that the humidity scale differs between campaigns.

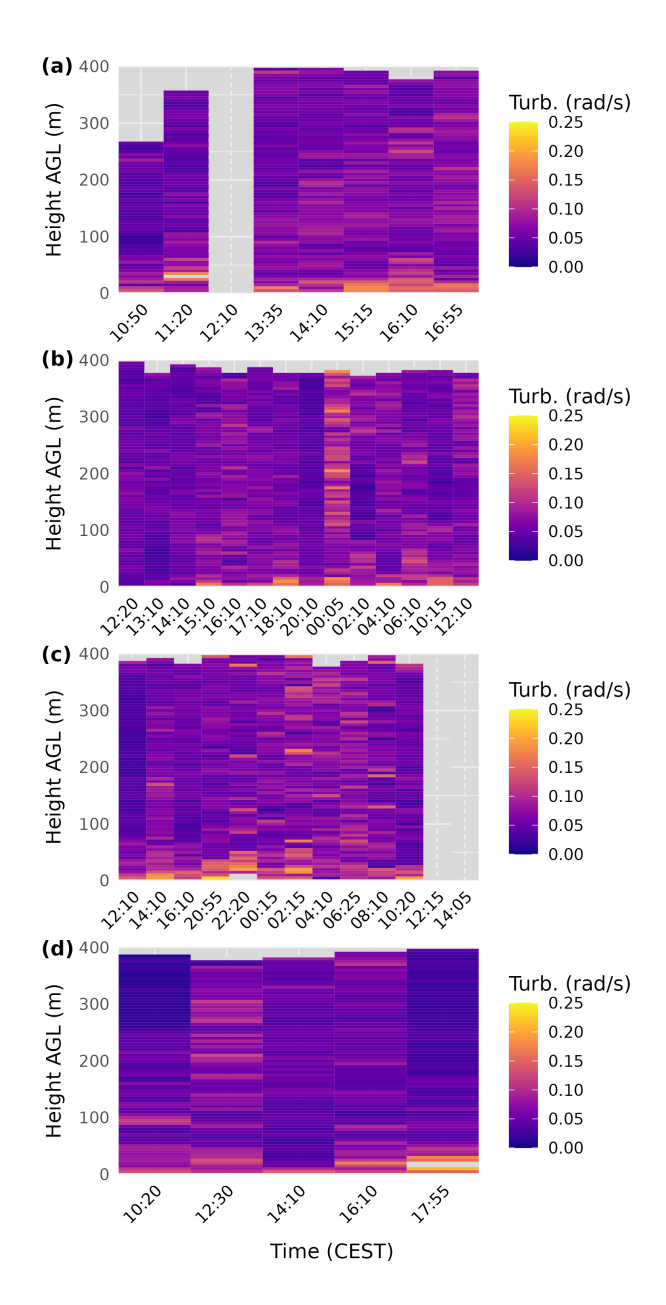


Figure 13. Course Heat maps of the temporal evolution of the estimated turbulence proxy over the tongue of the Kanderfirn on 16 June 2021 derived from the second descent of each UAV flight. The flight recorder file from during the 12 four measurement campaigns in 2021: 05-flight was corrupt 16 June (a), 9/10 July (b), 25/26 August (c), and could therefore not be analysed 23 September (d).

6 Discussion

430

435

440

450

455

The aim of the following discussion is (i) to outline the prospects and challenges of UAV-based atmospheric sounding in alpine terrain and (ii) to elaborate on the insights that the described measurement technique can provide into the local mountain-valley wind circulation and the structure of the atmospheric boundary layer over alpine glaciers.

6.1 Atmospheric sounding with UAVs in alpine terrain

The feasibility study and measurement campaign comprising four measurement campaigns on the Kanderfirn in the Swiss Alps on 16 June2021, 9/10 July, 25/26 August and 23 September has demonstrated the suitability of the developed low-cost and open-source fixed-wing UAV for atmospheric sounding of the boundary layer over alpine glaciers up to 800 m a.s.l. (Fig. D1). No major technical problems were encountered during the campaign. However, the campaign revealed some practical challenges and technical limitations that should be considered for future applications and the further development of the sounding technique presented. Manual take-off (i.e. hand launch) of fixed-wing UAVs above 2300 m a.s.l. is generally possible if a headwind, such as the persistent katabatic wind during the campaign, provides sufficient uplift. The downsite is that calm conditions increase the potential risk of a crash during launch at this altitude. In addition, hand launches require considerable experience and carry an inherent risk of injury. A much safer and more reliable technique for launching fixed-wing UAVs, which we have relied on in all subsequent campaigns to datehas been implemented successfully during the lat campaign, is the use of a bungee rope anchored to the glacier with an ice screw. The bungee rope is attached to a pin that is inserted into a small tube at the underside of the UAV and is automatically released when the UAV passes the anchor point. Due to the rough surface and presence of crevasses, moulins and meltwater channels, automatic landing of a fixed-wing UAVs on a glacier is very difficult. Manual landing is possible, but requires extensive training in the operation of fixed-wing UAVs.

Operating a fixed-wing UAV with a relatively large wingspan of 160 cm in alpine terrain has both advantages and disadvantages. Obviously, carrying a fixed-wing UAV of that size in alpine terrain is not convenient. However, the design of the fixed-wing UAV supports gliding and the operation at higher altitudes where air density is significantly reduced. Moreover, the large and coloured surface makes it possible to monitor the UAV at greater heights (up to several hundred metres above ground). This is important for safety reasons. In mountain ranges with heavy helicopter traffic, such as the Alps, automatic UAV operations may require manual intervention and sudden landings. In addition, UAV operations beyond visual line of sight are prohibited by most aviation authorities unless an exemption has been granted (EASA, 2023). Atmospheric soundings up to several hundred metres above ground are no longer possible in the Alps without special permission since the publication of the new EU drone regulations in January 2021, which limit the maximum flight height to 120m a.g.l. mAGL (note that the EU drone regulations were not yet in force in Switzerland during the campaign campaigns on the Kanderfirn in June 2021). Sounding the lowest 10-15 m a.g.l. is not practical with fixed-wing UAVs, as safe operation over rough surfaces cannot be guaranteed in either manual or automatic mode. In an ideal setup, atmospheric sounding with fixed-wing UAVs would be complemented by ground-based measurements (i.e. weather station and/or meteorological tower) and quadcopter soundings for the lowest tens of metres.

460 Compared to rotary-wing UAVs, where platform-induced heating can bias temperature measurements below the vehicle due to rotor downwash (e.g. Greene et al., 2018), the temperature and humidity sensor in the tube on the presented fixed-wing UAV is protected from solar radiation and major heat sources, and is naturally ventilated during flight. However, low ascent and descent rates are recommended to account for the effect of sensor inertia on air temperature and humidity measurements. Otherwise, the sensor time lag must be corrected (Reuder et al., 2009). While off-the-shelf UAVs usually do not support 465 the (easy) integration of scientific sensors and rather serve as a mobile platform for stand-alone sensors (e.g. Hansche et al., 2023; Messmer and Groos, 2024), UAVs tailored for scientific purposes, such as the presented fixed-wing UAV, support the integration of different sensors and allow the combined analysis of meteorological and flight recorder data (Reuder et al., 2009, 2012; Cassano et al., 2016). Flight recorder data are beneficial because they provide additional information to estimate atmospheric parameters such as wind speed, wind direction and turbulence, which go beyond the classical measurements of 470 air temperature and relative humidity (Mayer et al., 2012; Reuder et al., 2012; Cassano et al., 2016). However, a drawback of the presented sounding technique, which prevents easy replication, is the extensive training required to safely fly and land a fixed-wing UAV in alpine terrain. A more user-friendly system, especially for soundings in complex terrain, are hybrid UAVs that combine efficient forward flight with hovering and vertical take-off and landing capabilities. Hybrid UAVs for scientific research are currently under development, but still need to be tested in high mountain environments (Smeur et al., 2019; Bronz 475 et al., 2020).

6.2 Structure of the atmospheric Local circulations and boundary layer structure over alpine glaciers

480

490

The vertical profiles of air temperature, specific humidity, wind speed, wind direction and turbulence from Kanderfirn add to the sparse global dataset of atmospheric soundings over glacierised terrain and provide detailed insights into local circulations and the structure of the boundary layer over an alpine glacier during the early phase of the one ablation season. Apart from the Kanderfirn campaign, meteorological measurements with tethered balloons and UAVs up to a few hundred metres above the glacier surface are available from only four sites worldwide: From a glacio-meteorological field experiment on Pasterze in the Austrian Alps in summer 1994 (Van Den Broeke, 1997a, b; Oerlemans and Grisogono, 2002), from a glacio-meteorological field experiment on the Vatnajökull ice cap in Iceland in summer 1996 (Oerlemans et al., 1999), from a meteorological campaign on the Hofsjökull ice cap in Iceland in summer 2007 (Reuder et al., 2009, 2012), and from a field campaign on Mittivakkat Gletsjer in southeast Greenland in summer 2019 (Hansche et al., 2023). Although the topographical and climatic conditions vary greatly between the five sites, the soundings from the different campaigns reveal some general characteristics of the structure of the atmospheric boundary layer over glaciers and ice caps.

A key feature of the atmospheric boundary layer over mountain and outlet glaciers during the ablation season is the development of a cool and persistent density-driven katabatic wind. Katabatic winds have been observed during all of the summer field campaigns mentioned above, and are also evident in data from numerous on-glacier weather stations (e.g. Petersen and Pellicciotti, 2011; Petersen et al., 2013; Mott et al., 2020; Nicholson and Stiperski, 2020; Shaw et al., 2023, 2024). While measurements within the lowest metres above the glacier surface are crucial for investigating turbulent energy fluxes and determining the height of the maximum wind speed of the low-level katabatic jet (Van Den Broeke, 1997b; Oerlemans, 2010;

Mott et al., 2020; Nicholson and Stiperski, 2020), the vertical extent of the katabatic wind layer cannot be determined with weather stations and meteorological towers. The tethered alone, Tethered balloon and UAV soundings show that the katabatic wind layer is characterised by a pronounced surface-based inversion up to several tens of metres above the glacier surface (Van Den Broeke, 1997a; Oerlemans et al., 1999). While the maximum extension of the cooling effect of the katabatic wind layer has not been specifically investigated in previous studies (cf. Van Den Broeke, 1997a; Oerlemans et al., 1999; Hansche et al., 2023), the results from the Kanderfirn campaign show clearly that the top height of the surface-based inversion varies considerably in time and that the cooling effect at this location can reach up to 5060 m above the glacier surface (cf. Fig. ???9). The maximum cooling observed in the lowest 50 60 m of Kanderfirn was of the order of 4 °C in the late afternoon during the June campaign (cf. Fig. ??7a). This is in agreement consistent with theory, which predicts stronger katabatic winds for higher air temperatures outside the glacier that katabatic winds intensify with increasing temperature contrast between the glacier surface and its surroundings (Ohata, 1989; Oerlemans and Grisogono, 2002).

Besides the pronounced cooling effect, relatively dry air, high wind speeds and enhanced turbulence characterise the katabatic wind layer over glaciers during the ablation season. A dry surface layer and a marked increase in humidity in the first tens of metres above the glacier surface, such as observed on Kanderfirn during the June campaign (cf. Fig. ??7a), were also found on Pasterze and Mittivakkat Gletsjer (Van Den Broeke, 1997a; Hansche et al., 2023). Since the specific humidity on the Kanderfirn was higher throughout the sounded air column above the katabatic wind layer, it is very likely that the dry air near the glacier surface originates from the accumulation area, where evaporation is limited compared to the ablation zone, or from the free atmosphere above. The saturation deficit caused by the dry low-level jet, together with relatively high wind speeds and increased turbulence, may favour evaporation and thus reduce the energy available for melting snow and ice in the ablation zone. This means that katabatic flow has the potential to reduce not only the sensible heat flux (e.g. Shaw et al., 2024), but also the latent heat flux compared to the microclimatic conditions (warmer and more humid air) outside the glacier under certain synoptic situations. Since the temperature and humidity profiles observed above the top height of the surface-based inversions are linear (Figs. ?? and ??; Oerlemans et al., 1999)(Figs. 7 and C1; Oerlemans et al., 1999), their extrapolation to the glacier surface and deviation from the measurements below the inversion top height provide an alternative to off-glacier lapse rates and gradients (see e.g. Greuell and Böhm, 1998; Shea and Moore, 2010; Shaw et al., 2024) for estimating and parameterising the cooling and drying effect of the katabatic wind layer.

Above the katabatic wind layer, a well-developed mountain-valley wind circulation similar to that at Kanderfirm on Kanderfirm (cf. Fig. 8c,d) has been found at Pasterze and Vatnajökull during periods of stable weather (Van Den Broeke, 1997b; Oerlemans et al., 1999). A characteristic feature is the decrease in wind speed from a maximum near the surface to a minimum at about 100-200 m above the surface (cf. Fig. ??8c). At the height of the minimum wind speed, the horizontal wind direction changes from downglacier to upglacier (Fig. ??; Van Den Broeke, 1997b) down-glacier to up-glacier (Fig. 8d; Van Den Broeke, 1997b). The valley wind typically advects warmer and more humid air towards the glacier (Figs. ?? and ??; Van Den Broeke, 1997b) (Van Den Broeke, 1997b). However, without additional atmospheric soundings along the glacier flow line, it is difficult to assess whether the glacier and valley winds are essentially decoupled during stable conditions such as on 16 June 2021, or whether entrainment of warm and humid air occurs at higher altitudes. To better capture the interactions between the differ-

ent thermally driven winds in glacierised alpine terrain, parallel UAV-based atmospheric soundings at different locations on the glacier, together with ground-based measurements, would be helpful. Repeating such soundings under different synoptic conditions would help to identify the atmospheric conditions that favour the decay of the katabatic wind layer and the heat advection from outside the glacier. This information is crucial to improve the parameterisation of local atmospheric conditions over mountain glaciers and to assess how a warming world affects the local circulation in alpine terrain.

7 Conclusions

530

555

With the UAV-based atmospheric sounding technique, we have presented a new approach to study the interaction of local winds in alpine terrain and investigate the structure of the atmospheric boundary layer over glaciers up to several hundred metres above the surface. The measurement technique provides a lightweight and low-cost alternative to tethered balloons and complements ground-based measurements at weather stations and meteorological towers. Vertical profiles of air temperature, humidity, pressure, wind speed, wind direction and turbulence can be derived from the synchronised meteorological and flight recorder data collected by the developed open-source fixed-wing UAV. A drawback of the fixed-wing UAV is the extensive 540 training that is required for safe operation in alpine terrain. However, a hybrid UAV combining efficient forward flight with hovering and vertical take-off and landing capabilities is currently under development and will facilitate enhance operation in alpine terrain. The UAV-based atmospheric soundings conducted during the feasibility study at the Kanderfirn in the Swiss Alps add to the sparse global dataset of atmospheric soundings in glacierised terrain and reveal typical features of the boundary 545 layer over glaciers in summer. A persistent low-level katabatic jetglacier wind, characterised by a pronounced surface-based inversion, relatively dry air, high wind speeds and enhanced turbulence, was observed at the Kanderfirn. Above the katabatic wind layer, a well-developed valley wind adevecting warm and humid air from the periphery towards the glacier was found. While vertical profiles at one location can provide fundamental insights into the structure of the boundary layer over glaciers, parallel UAV-based soundings at different locations and repeated under different synoptic conditions would be desirable in the future to uncover the interactions between the thermally driven local winds in alpine terrain and to assess the potential 550 impact of rising off-glacier temperatures on the katabatic wind and its wider cooling effect of the katabatic wind specifically and on the local circulations in alpine terrain in general.

Code and data availability. The atmospheric sounding and flight recorder data as well as the scripts for data post-processing, reformatting, analysis and visualisation can be downloaded from the open-access repository Zenodo: https://doi.org/10.5281/zenodo.13889613 (Groos et al., 2024). The mobile measurement post-processing (mmp) FORTRAN package can be downloaded from the following Git repository: https://git.rz.uni-augsburg.de/philipan/mmp (Philipp, 2024).

Author contributions. ARG conceived the study. ARG and AP designed the UAV. MB supported the development of the UAS and helped to implement the Paparazzi UAV software and hardware. NB built the two UAVs with the help of ARG. NB and ARG carried out the mea-

surement campaign. AP developed the mmp software package for processing and analysing the flight data and atmospheric measurements.

ARG, NB and AP analysed the data. ARG drafted the manuscript and prepared the figures with contributions from NB and AP. All authors contributed to the discussion of the results and revision of the manuscript.

Competing interests. The authors declare that they have no competing interests.

Acknowledgements. The expenses for the construction of the fixed-wing UAVs and the implementation of the measurement campaign on the Kanderfirn were covered by the Institute of Geography of the University of Bern. We would like to thank Heinz Veit for the support of this study and Peter Leiser for his help in soldering the electronic components of the two UAVs. Moreover, we wish to extend our gratitude to the other lead developers of the Paparazzi UAV project (namely Gautier Hattenberger and Hector Garcia de Marina) for the fruitful discussions and their support in implementing the UAV hardware and ground control station software.

Appendix A: Sensor intercomparison

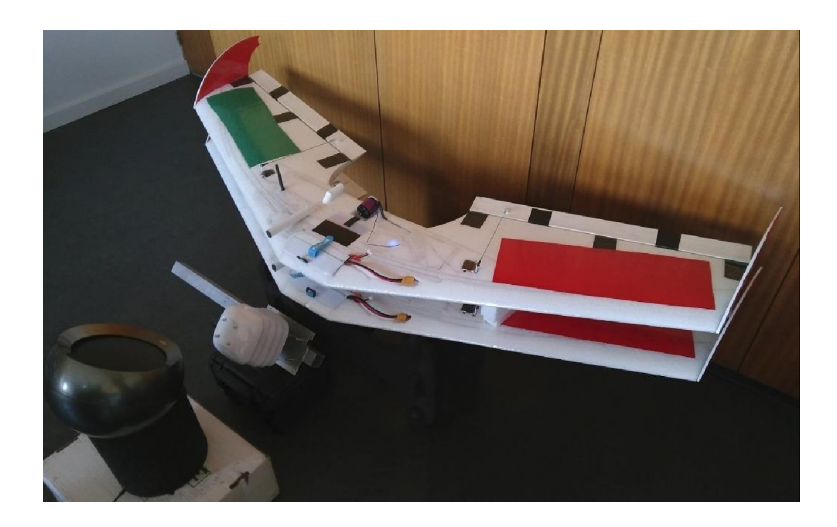


Figure A1. Setup of the 24-hour intercomparison measurement of the temperature and humidity sensors (SHT75) installed inside the white tube of each UAV and a reference sensor (SHT21, inside the radiation shield) placed in front of both UAVs. A fan ensured continuous air flow. The experiment was conducted from 4 to 5 June 2021.

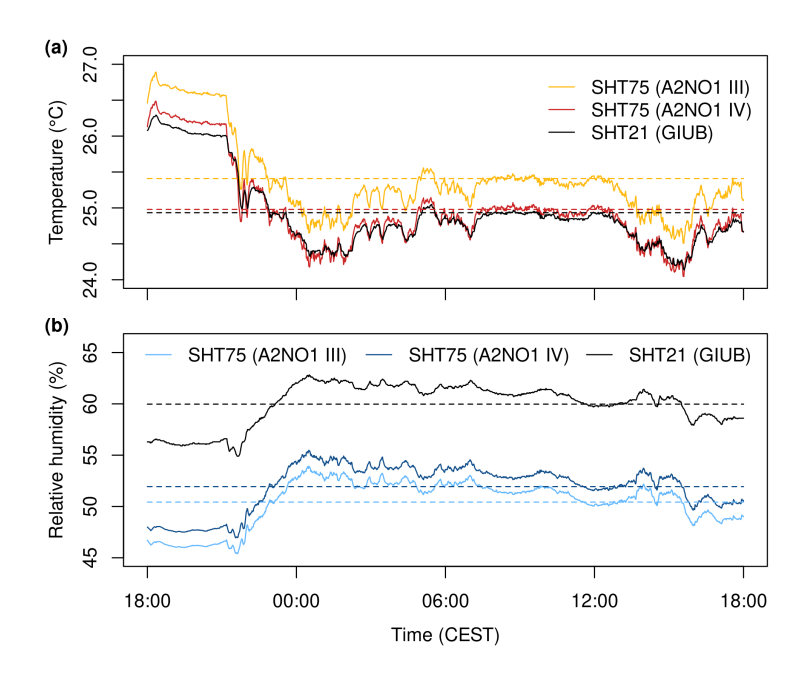


Figure A2. Result of the 24-hour intercomparison measurement. The mean difference in air temperature between both SHT75 sensors is 0.43 °C and the mean difference in relative humidity is 1.5 %.

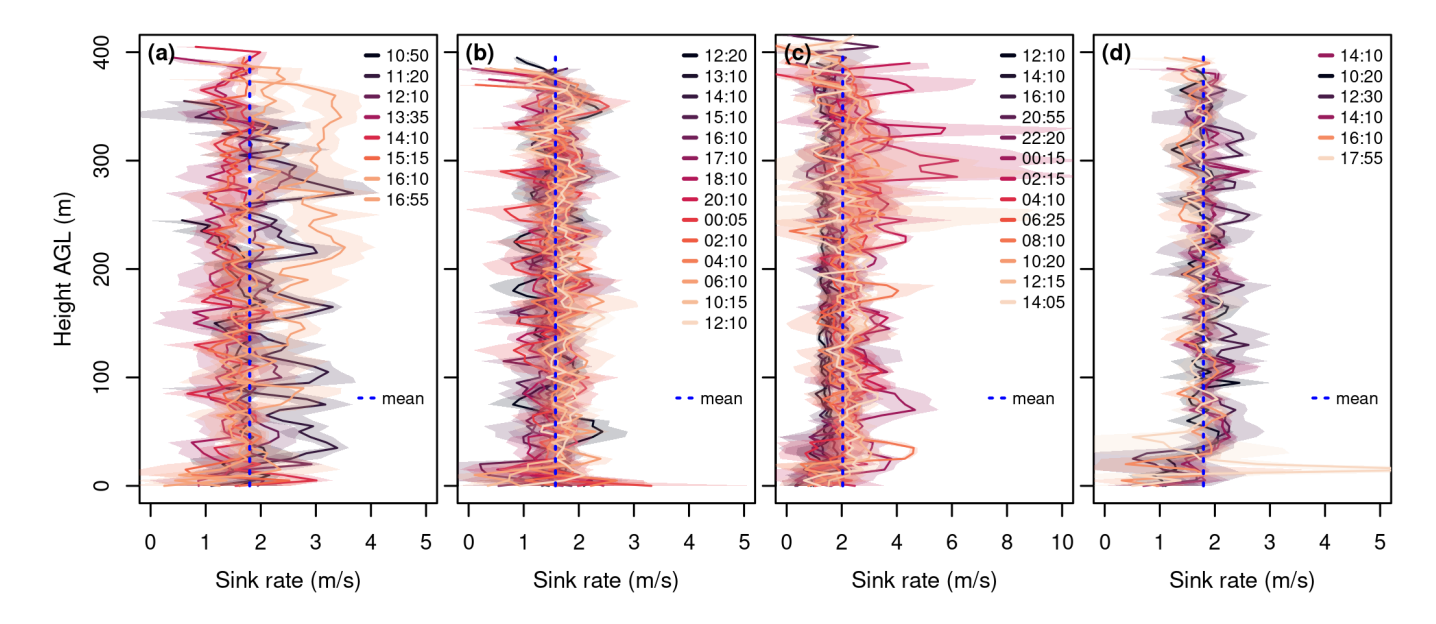


Figure B1. Example of the derivation of the lapse Sink rate over the Kanderfirn and the surrounding area for (binned into 5 m height intervals) from all soundings (each consisting of two descents) on 16 June 2021 at about 14:10. (a) Lapse rate below and above the top height of the surface-based inversion derived from the UAV-based atmospheric soundings., 9/10 July (b) Environmental lapse rate in the study., 25/26 August (c), and 23 September 2021 (d). The shaded area derived from represents the data of three nearby weather stations standard deviation between the two descents.

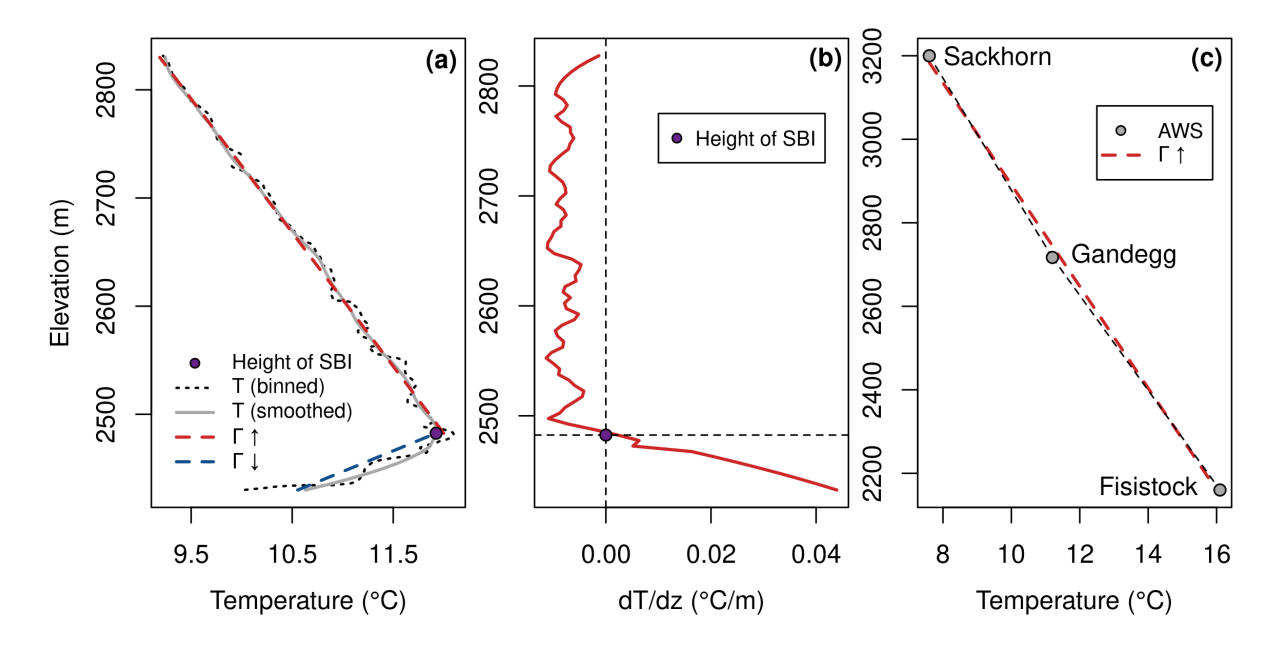


Figure C1. Example of the derivation of the lapse rate over the Kanderfirn and its surroundings on 16 June 2021 at about 14:10. (a) Lapse rate below (Γ_{\downarrow}) and above (Γ_{\uparrow}) the top height of the surface-based inversion (SBI) derived from UAV-based atmospheric soundings. (b) First derivative of the smoothed air temperature profile with respect to altitude; the altitude where the derivative becomes positive defines the top height of the SBI. (c) Environmental lapse rate in the study area derived from three nearby weather stations.

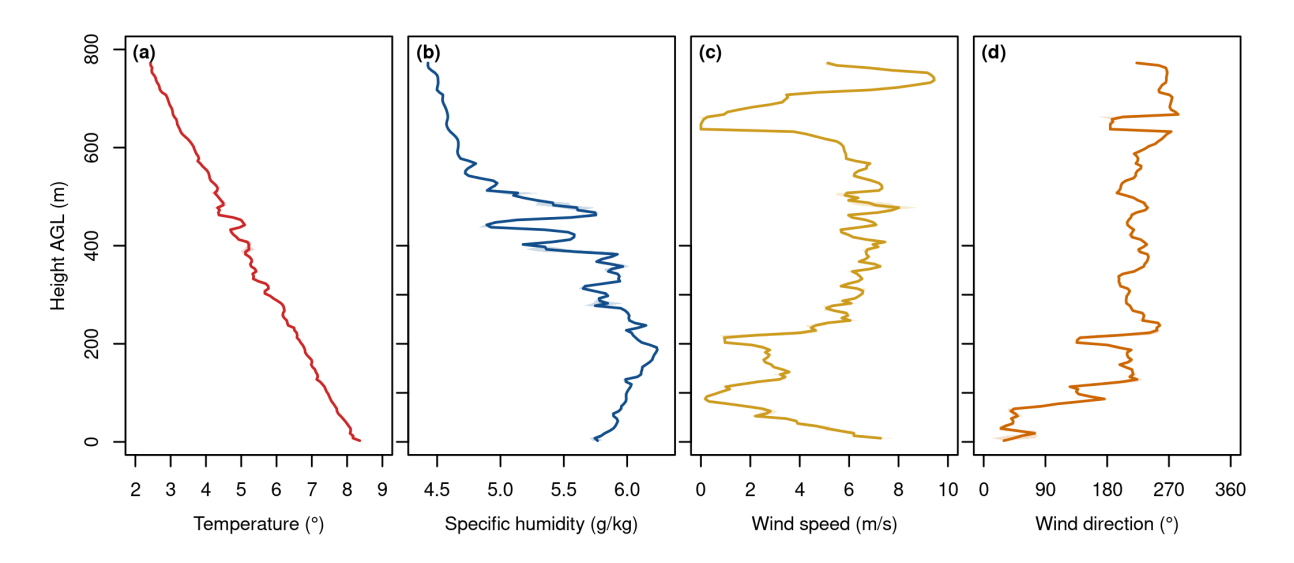


Figure D1. Synthesis plot showing air temperature (a), specific humidity (b), wind speed (c), and wind direction (d) profiles from the 800 m sounding on 26 August 2021 at about 14:05.

References

590

- Bonin, T. A., Chilson, P. B., Zielke, B. S., Klein, P. M., and Leeman, J. R.: Comparison and application of wind retrieval algorithms for small unmanned aerial systems, Geoscientific Instrumentation, Methods and Data Systems, 2, 177–187, https://doi.org/10.5194/gi-2-177-2013, 2013.
 - Bronz, M., Tal, E., Favalli, F., and Karaman, S.: Mission-Oriented Additive Manufacturing of Modular Mini-UAVs, in: AIAA Scitech 2020 Forum, pp. 1–11, American Institute of Aeronautics and Astronautics, Orlando, FL, https://doi.org/10.2514/6.2020-0064, 2020.
 - Cassano, J. J.: Observations of atmospheric boundary layer temperature profiles with a small unmanned aerial vehicle, Antarctic Science, 26, 205–213, https://doi.org/10.1017/S0954102013000539, 2014.
- Cassano, J. J., Seefeldt, M. W., Palo, S., Knuth, S. L., Bradley, A. C., Herrman, P. D., Kernebone, P. A., and Logan, N. J.: Observations of the atmosphere and surface state over Terra Nova Bay, Antarctica, using unmanned aerial systems, Earth System Science Data, 8, 115–126, https://doi.org/10.5194/essd-8-115-2016, 2016.
 - DWD: Aspirations-Psychrometer-Tafeln, Vieweg & Sohn Verlagsgesellschaft, Braunschweig, 1976.
 - EASA: Guidelines for UAS operations in the open and specific category Ref to Regulation (EU) 2019/947, 2023.
- Farina, S. and Zardi, D.: Understanding Thermally Driven Slope Winds: Recent Advances and Open Questions, Boundary-Layer Meteorology, 189, 5–52, https://doi.org/10.1007/s10546-023-00821-1, 2023.
 - Greene, B. R., Segales, A. R., Waugh, S., Duthoit, S., and Chilson, P. B.: Considerations for temperature sensor placement on rotary-wing unmanned aircraft systems, Atmospheric Measurement Techniques, 11, 5519–5530, https://doi.org/10.5194/amt-11-5519-2018, 2018.
 - Greuell, W. and Böhm, R.: 2 m temperatures along melting mid-latitude glaciers, and implications for the sensitivity of the mass balance to variations in temperature, Journal of Glaciology, 44, 9–20, https://doi.org/10.3189/S0022143000002306, 1998.
 - Groos, A. R., Bertschinger, T. J., Kummer, C. M., Erlwein, S., Munz, L., and Philipp, A.: The potential of low-cost UAVs and open-source photogrammetry software for high-resolution monitoring of alpine glaciers: A case study from the Kanderfirn (Swiss Alps), Geosciences, 9, 1–21, https://doi.org/10.3390/geosciences9080356, 2019.
- Groos, A. R., Aeschbacher, R., Fischer, M., Kohler, N., Mayer, C., and Senn-Rist, A.: Accuracy of UAV Photogrammetry in Glacial and Periglacial Alpine Terrain: A Comparison With Airborne and Terrestrial Datasets, Front. Remote Sens. Frontiers in Remote Sensing, 3, 16, https://doi.org/10.3389/frsen.2022.871994, 2022.
 - Groos, A. R., Brand, N., Bronz, M., and Philipp, A.: Atmospheric sounding of the boundary layer over alpine glaciers using fixed-wing UAVs (v1.0.0) [Data set], Zenodo, https://doi.org/10.5281/zenodo.13889613, 2024.
 - Hansche, I., Shahi, S., Abermann, J., and Schöner, W.: The vertical atmospheric structure of the partially glacierised Mittivakkat valley, southeast Greenland, Journal of Glaciology, 69, 1097–1108, https://doi.org/10.1017/jog.2022.120, 2023.
 - Hattenberger, G., Bronz, M., and Gorraz, M.: Using the Paparazzi UAV System for Scientific Research, in: IMAV 2014, International Micro Air Vehicle Conference and Competition (Delft, Netherlands: Delft University of Technology), pp. 247–252, https://doi.org/10.4233/uuid:b38fbdb7-e6bd-440d-93be-f7dd1457be60, 2014.
- Huss, M. and Hock, R.: Global-scale hydrological response to future glacier mass loss, Nature Climate Change, https://doi.org/10.1038/s41558-017-0049-x, 2018.
 - Jonassen, M. O., Tisler, P., Altstädter, B., Scholtz, A., Vihma, T., Lampert, A., König-Langlo, G., and Lüpkes, C.: Application of remotely piloted aircraft systems in observing the atmospheric boundary layer over Antarctic sea ice in winter, Polar Research, 34, 25651, https://doi.org/10.3402/polar.v34.25651, 2015.

- Jouberton, A., Shaw, T. E., Miles, E., McCarthy, M., Fugger, S., Ren, S., Dehecq, A., Yang, W., and Pellicciotti, F.: Warming-induced monsoon precipitation phase change intensifies glacier mass loss in the southeastern Tibetan Plateau, Proceedings of the National Academy of Sciences, 119, e2109796119, https://pnas.org/doi/full/10.1073/pnas.2109796119, 2022.
 - Lampert, A., Altstädter, B., Bärfuss, K., Bretschneider, L., Sandgaard, J., Michaelis, J., Lobitz, L., Asmussen, M., Damm, E., Käthner, R., Krüger, T., Lüpkes, C., Nowak, S., Peuker, A., Rausch, T., Reiser, F., Scholtz, A., Sotomayor Zakharov, D., Gaus, D., Bansmer, S., Wehner, B., and Pätzold, F.: Unmanned Aerial Systems for Investigating the Polar Atmospheric Boundary Layer—Technical Challenges and Examples of Applications, Atmosphere, 11, 416, https://doi.org/10.3390/atmos11040416, 2020.

615

- Litt, M., Sicart, J.-E., and Helgason, W.: A study of turbulent fluxes and their measurement errors for different wind regimes over the tropical Zongo Glacier (16° S) during the dry season, Atmospheric Measurement Techniques, 8, 3229–3250, https://doi.org/10.5194/amt-8-3229-2015, 2015.
- Mayer, S., Hattenberger, G., Brisset, P., Jonassen, M., and Reuder, J.: A 'no-flow-sensor' wind estimation algorithm for unmanned aerial systems, International Journal of Micro Air Vehicles, 4, 15–30, 2012.
- Messmer, J. and Groos, A. R.: A low-cost and open-source approach for supraglacial debris thickness mapping using UAV-based infrared thermography, The Cryosphere, 18, 719–746, https://doi.org/10.5194/tc-18-719-2024, 2024.
- Mott, R., Stiperski, I., and Nicholson, L.: Spatio-temporal flow variations driving heat exchange processes at a mountain glacier, The Cryosphere, 14, 4699–4718, https://doi.org/10.5194/tc-14-4699-2020, 2020.
- Nicholson, L. and Stiperski, I.: Comparison of turbulent structures and energy fluxes over exposed and debris-covered glacier ice, Journal of Glaciology, pp. 1–13, https://doi.org/10.1017/jog.2020.23, 2020.
 - Oerlemans, J.: The Microclimate of Valley Glaciers, Igitur, Utrecht Publishing & Archiving Services, Universiteitsbibliotheek Utrecht, 2010.
 - Oerlemans, J. and Grisogono, B.: Glacier winds and parameterisation of the related surface heat fluxes, Tellus A: Dynamic Meteorology and Oceanography, 54, 440, https://doi.org/10.3402/tellusa.v54i5.12164, 2002.
- Oerlemans, J. and Vugts, H. F.: A Meteorological Experiment in the Melting Zone of the Greenland Ice Sheet, Bulletin of the American Meteorological Society, 74, 355–365, https://doi.org/10.1175/1520-0477(1993)074<0355:AMEITM>2.0.CO;2, 1993.
 - Oerlemans, J., Björnsson, H., Kuhn, M., Obleitner, F., Palsson, F., Smeets, C., Vugts, H. F., and Wolde, J. D.: Glacio-Meteorological Investigations On Vatnajökull, Iceland, Summer 1996: An Overview, Boundary-Layer Meteorology, 92, 3–24, https://doi.org/10.1023/A:1001856114941, 1999.
- Ohata, T.: Katabatic Wind on Melting Snow and Ice Surfaces (II): Application of a Theoretical Model, Journal of the Meteorological Society of Japan. Ser. II, 67, 113–122, https://doi.org/10.2151/jmsj1965.67.1_113, 1989.
 - Petersen, L. and Pellicciotti, F.: Spatial and temporal variability of air temperature on a melting glacier: Atmospheric controls, extrapolation methods and their effect on melt modeling, Juncal Norte Glacier, Chile: TEMPERATURE VARIABILITY OVER A GLACIER, Journal of Geophysical Research: Atmospheres, 116, n/a–n/a, https://doi.org/10.1029/2011JD015842, 2011.
- Petersen, L., Pellicciotti, F., Juszak, I., Carenzo, M., and Brock, B.: Suitability of a constant air temperature lapse rate over an Alpine glacier: testing the Greuell and Böhm model as an alternative, Annals of Glaciology, 54, 120–130, https://doi.org/10.3189/2013AoG63A477, 2013.
 - Philipp, A.: mmp mobile measurement post-processing [Software package], GitLab University of Augsburg, https://git.rz.uni-augsburg.de/philipan/mmp, 2024.
- Potter, E. R., Orr, A., Willis, I. C., Bannister, D., and Salerno, F.: Dynamical Drivers of the Local Wind Regime in a Himalayan Valley, Journal of Geophysical Research: Atmospheres, 123, 13,186–13,202, https://doi.org/10.1029/2018JD029427, 2018.

- Reuder, J., Brisset, P., Jonassen, M., Müller, M., and Mayer, S.: The Small Unmanned Meteorological Observer SUMO: A new tool for atmospheric boundary layer research, Meteorologische Zeitschrift, 18, 141–147, https://doi.org/10.1127/0941-2948/2009/0363, 2009.
- Reuder, J., Ablinger, M., Ágústsson, H., Brisset, P., Brynjólfsson, S., Garhammer, M., Jóhannesson, T., Jonassen, M. O., Kühnel, R., Lämm lein, S., De Lange, T., Lindenberg, C., Malardel, S., Mayer, S., Müller, M., Ólafsson, H., Rögnvaldsson, O., Schäper, W., Spengler, T.,
 Zängl, G., and Egger, J.: FLOHOF 2007: an overview of the mesoscale meteorological field campaign at Hofsjökull, Central Iceland,
 Meteorology and Atmospheric Physics, 116, 1–13, https://doi.org/10.1007/s00703-010-0118-4, 2012.
 - Rounce, D. R., Hock, R., Maussion, F., Hugonnet, R., Kochtitzky, W., Huss, M., Berthier, E., Brinkerhoff, D., Compagno, L., Copland, L., Farinotti, D., Menounos, B., and McNabb, R. W.: Global glacier change in the 21st century: Every increase in temperature matters, Science, 379, 78–83, https://doi.org/10.1126/science.abo1324, 2023.

- Salerno, F., Guyennon, N., Yang, K., Shaw, T. E., Lin, C., Colombo, N., Romano, E., Gruber, S., Bolch, T., Alessandri, A., Cristofanelli, P., Putero, D., Diolaiuti, G., Tartari, G., Verza, G., Thakuri, S., Balsamo, G., Miles, E. S., and Pellicciotti, F.: Local cooling and drying induced by Himalayan glaciers under global warming, Nature Geoscience, 16, 1120–1127, https://doi.org/10.1038/s41561-023-01331-y, 2023.
- Savitzky, A. and Golay, M. J. E.: Smoothing and Differentiation of Data by Simplified Least Squares Procedures, Analytical Chemistry, 36, 1627–1639, https://doi.org/10.1021/ac60214a047, 1964.
 - Shaw, T. E., Brock, B. W., Fyffe, C. L., Pellicciotti, F., Rutter, N., and Diotri, F.: Air temperature distribution and energy-balance modelling of a debris-covered glacier, Journal of Glaciology, 62, 185–198, https://doi.org/10.1017/jog.2016.31, 2016.
- Shaw, T. E., Brock, B. W., Ayala, A., Rutter, N., and Pellicciotti, F.: Centreline and cross-glacier air temperature variability on an Alpine glacier: assessing temperature distribution methods and their influence on melt model calculations, Journal of Glaciology, 63, 973–988, https://doi.org/10.1017/jog.2017.65, 2017.
 - Shaw, T. E., Yang, W., Ayala, A., Bravo, C., Zhao, C., and Pellicciotti, F.: Distributed summer air temperatures across mountain glaciers in the south-east Tibetan Plateau: temperature sensitivity and comparison with existing glacier datasets, The Cryosphere, 15, 595–614, https://doi.org/10.5194/tc-15-595-2021, 2021.
- 670 Shaw, T. E., Buri, P., McCarthy, M., Miles, E. S., Ayala, A., and Pellicciotti, F.: The Decaying Near-Surface Boundary Layer of a Retreating Alpine Glacier, Geophysical Research Letters, 50, e2023GL103 043, https://doi.org/10.1029/2023GL103043, 2023.
 - Shaw, T. E., Buri, P., McCarthy, M., Miles, E. S., and Pellicciotti, F.: Local Controls on Near-Surface Glacier Cooling Under Warm Atmospheric Conditions, Journal of Geophysical Research: Atmospheres, 129, e2023JD040214, https://doi.org/10.1029/2023JD040214, 2024.
- Shea, J. M. and Moore, R. D.: Prediction of spatially distributed regional-scale fields of air temperature and vapor pressure over mountain glaciers, Journal of Geophysical Research: Atmospheres, 115, 2010JD014351, https://doi.org/10.1029/2010JD014351, 2010.
 - Smeur, E. J. J., Bronz, M., and de Croon, G. C. H. E.: Incremental Control and Guidance of Hybrid Aircraft Applied to a Tailsitter Unmanned Air Vehicle, Journal of Guidance, Control, and Dynamics, 43, 274–287, https://doi.org/10.2514/1.G004520, 2019.
- Steiner, J. F. and Pellicciotti, F.: Variability of air temperature over a debris-covered glacier in the Nepalese Himalaya, Annals of Glaciology, 57, 295–307, https://doi.org/10.3189/2016AoG71A066, 2016.
 - Van Den Broeke, M. R.: Momentum, Heat, and Moisture Budgets of the Katabatic Wind Layer over a Midlatitude Glacier in Summer, Journal of Applied Meteorology, 36, 763–774, https://doi.org/10.1175/1520-0450(1997)036<0763:MHAMBO>2.0.CO;2, 1997a.
 - Van Den Broeke, M. R.: Structure and diurnal variation of the atmospheric boundary layer over a mid-latitude glacier in summer, Boundary-Layer Meteorology, 83, 183–205, https://doi.org/10.1023/A:1000268825998, 1997b.